DOE/ER/14083-2
ESL-93033-TR

# TENSOR CONTROLLED-SOURCE AUDIOMAGNETOTELLURIC SURVEY OVER THE SULPHUR SPRINGS THERMAL AREA, VALLES CALDERA, NEW MEXICO, U. S.A.; IMPLICATIONS FOR STRUCTURE OF THE WESTERN CALDERA AND FOR CSAMT METHODOLOGY

Final Report to

United States Department of Energy
Office of Basic Energy Sciences
Division of Geosciences

by

Philip E. Wannamaker



**Earth Science Laboratory**

**University of Utah Research Institute**
391 Chipeta Way, Suite C
Salt Lake City, Utah 84108-1292
(801) 584-4422

June, 1994

DOE/ER/14083-2
ESL-93033-TR

# TENSOR CONTROLLED-SOURCE AUDIOMAGNETOTELLURIC SURVEY OVER THE SULPHUR SPRINGS THERMAL AREA, VALLES CALDERA, NEW MEXICO, U. S. A.; IMPLICATIONS FOR STRUCTURE OF THE WESTERN CALDERA AND FOR CSAMT METHODOLOGY

Final Report to

United States Department of Energy
Office of Basic Energy Sciences
Division of Geosciences

by

Philip E. Wannamaker

Earth Science Laboratory
University of Utah Research Institute
391 Chipeta Way, Suite C
Salt Lake City, Utah 84108-1295

June, 1994

## ABSTRACT

We have carried out an extensive tensor CSAMT survey of the Sulphur Springs geothermal area, Valles Caldera, New Mexico. This survey, consisting of 45 high-quality sites, has been acquired by in support of Continental Scientific Drilling Program (CSDP) drillholes VC-2A and VC-2B. Two independent transmitter dipoles were energized for tensor measurements using a 30 kW generator placed approximately 13 km south of the VC-2B wellhead. The soundings in the Sulphur Springs area were arranged in four profiles to cross major structural features. The electric bipoles parallel to each profile were deployed contiguously to ensure against spatial aliasing of the impedance response corresponding to current flow across structural trends. The frequency range of acquisition was 4096 Hz down to 1 Hz for the central line, but only down to 4 Hz for most sites of the other lines. Data quality is high overall and is established by repeatability of measurements. Agreement between the CSAMT amd available natural field MT data is very good over almost all the period range of overlap indicating that we are free of calibration problems and that far-field results are generally being obtained. Non plane-wave effects in the CSAMT around Sulphur Springs are apparent at 1 to 2 Hz, and perhaps slightly even at 4 Hz, however, which is near the bottom of our frequency range.

CSAMT and MT data taken outside the Valles Caldera to the west were modeled in an attempt to compare resistivity structure exterior to the caldera to that within. The model of the external data consists of a few hundred meters of resistive (200 - 400 ohm-m) Bandelier Tuff, underlain by conductive Paleozoic sedimentary rocks (nominally 240 m of 10 ohm-m), and further underlain by resistive (greater than 200 ohm-m), primarily Precambrian crystalline rocks. Derivation of model resistivity cross sections from our data profiles interior to the caldera procedes through constrained trial-and-error forward modeling and parameterized inversion of two-dimensional (2-D) resistivity cross sections. To date, a final model has been derived for the central, longest profile straddling corehole VC-2B, whose lithologic log is very valuable in relating resistivity structure to geology. East of Sulphur Creek fault, the upper 200m of the section is of relatively low resistivity (5 - 30 ohm-m) and corresponds to unconsolidated landslide and debris flows. In the depth interval 200 to 750 m east of Sulphur Creek fault, the substantially welded Bandelier Tuff sequence exhibits relatively high resistivities (200 - 300 ohm-m), similar in values to those reported for electric logs from the Redondo Graben area and to those interpreted from the CSAMT data exterior to the caldera. Below the Bandelier Tuff, the Paleozoic sedimentary layer is of only somewhat lower resistivity (about 5 - 8 ohm-m) than it is to the west outside the caldera, perhaps related to hydrothermal activity. Toward the east end of the profile, evidence for this sedimentary layer disappears, in apparent keeping with structural interpretations of a substantial downdrop of the section to the east across the Freelove Canyon normal fault. At depths beyond about 1500 m below the surface, MT data near well VC-2B imply resistive basement corresponding to the crystalline Precambrian. No particularly high resistivities possibly corresponding to a vapor zone in the upper 500 m near VC-2B implied from acid-sulphate alteration and subhydrostatic well pressures are evident in the CSAMT data. However, the Sulphur Creek fault itself appears to be a locus of substantial change in structural relief; upthrow of stratigraphy and basement to its west appears to be about 400 - 500 m. No further structural relief is detected west of Sulphur Creek fault. This is at variance with published geologic cross sections based on sparse drilling data and surface mapping, which show a nearly continuous distribution of normal faulting but which are

poorly constrained in this area.

With the availability of tensor CSAMT and MT data both inside and outside Valles Caldera, assumptions and methods of CSAMT can be tested. For example, one-dimensional inversion of CSAMT and MT data at a site outide the caldera about 10 km from the transmitter indicate that non plane-wave effects enter this data at 8 Hz and lower frequencies. Implied penetration depths at 8 Hz are only about 1/20th of the transmitter-receiver separation, which is much more pessimistic than traditional assumptions about available depth of exploration in the plane-wave regime (usually 1/5th the separation or more). This is interpreted to result from transmitter EM fields entering the basement in the vicinity of the transmitter and propogating to the receiver with relatively little attenuation. Furthermore, comparison of observed electric (E) and magnetic (H) fields at this site with those computed from the layered resistivity model derived from 1-D inversion of the apparent resistivity and impedance phase can provide information about structure below the transmitter site. Small, frequency-independent shifts (about 0.1 log unit) down to about 8 Hz in the fields indicate that very small-scale, local structure does not lead to transmitter overprint effects in the impedance data at the receiver but instead acts as an equivalent far-field source. Below 8 Hz, however, the observed E and H fields fall substantially below those computed from the layered model and suggest structure of several kilometers scale around the transmitter may be conductive relative to the receiver.

In the Sulphur Springs area, near-coincident CSAMT and MT data near well VC-2B indicate that non plane-wave effects in the apparent resistivity and impedance phase occur at a frequency near to that predicted from the resistivity structure local to the western caldera. This is confirmed by interpretation of the electric and magnetic fields; their amplitudes suggest an effective regional layered host with an upper resistive volcanic section like the Bandelier Tuff, underlain by conductive layering like the Paleozoic sediments of the western caldera, and a resistive basal half-space presumably representing the crystalline Precambrian. Major and minor ellipse axes for the observed E and H field data are defined and compared to those computed theoretically from fields using the effective layered model of regional resistivity. The study suggests more generally that one might define an effective regional host using just the magnetic field, thereby allowing correction for near-field effects in the CSAMT data. For the magnetic fields especially, agreement between observed and computed ellipse axes is quite close over the entire survey area, suggesting that no large-scale inhomogeneity is distorting incident field orientation and azimuth. The observed electric fields are much more strongly affected by geology. Numerous and sometimes strong, site-to-site variations due to small-scale structure are evident also. When heterogeneity of any scale is important, significant departures between scalar and vector CSAMT data can be expected, and are observed in this survey. Scalar data ignore the contributions by the on-diagonal elements of the tensor impedance and this effect is exacerbated when the source field is poorly coupled to the sensors. This problem should be much reduced for vector CSAMT measurements where all horizontal field components are measured and the maximally-coupled results are defined.

# INTRODUCTION

Electrical resistivity is being recognized increasingly as a unique window on earth processes and resources (Wannamaker and Hohmann, 1991). One of the most widely applied approaches for resolving resistivity structure is estimation of the plane-wave EM impedance of the earth, e.g., magnetotellurics (MT) and related methods. In this approach, the source EM fields do not decay geometrically with depth, only dissipatively, which tends to improve resolution vertically. In addition, measurement of the electric field component also improves resolution, especially laterally, provided it is properly interpreted. Finally, the state of the art in multi-dimensional EM response modeling and inversion is relatively well advanced for plane-wave methods.

For exploration scales limited to the upper 2 km or so of the earth (frequencies from one or a few Hertz to perhaps 10 kHz), it is considered practical to generate planar EM fields using distant artificial current sources. This is the controlled-source audiomagnetotelluric (CSAMT) technique (Goldstein and Strangway, 1975; Zonge and Hughes, 1991). Such an approach has been extensively used for exploration problems in geothermal (e.g., Sandberg and Hohmann, 1982; Bartel and Jacobsen, 1987), precious metal (Corbett, 1991; Wilds and MacInnes, 1991), and hydrocarbon (Hughes and Carlson, 1987; Ostrander, 1990) environments. Many other case histories including sulfide exploration, mapping of brine plumes, and geotechnical applications are reviewed by Zonge and Hughes (1991).

One major difference between typical natural-field MT and CSAMT procedures is the much-simplified, scalar approach typical of the latter measurement. Tensor data has been considered essential for MT for over thirty years now due to recognized inhomogeneity in the earth and temporal variations in the natural field polarizations. Scalar measurements have been taken for CSAMT due often to cost considerations and perhaps to the assumption that responses from the upper 1-2 km are less inhomogeneous than crustal-scale responses, and that dense coverage by scalar measurements should be sufficient to constrain lateral structure. Since the reputation of a geophysical method depends on its accuracy and reliability, a detailed comparison of the rigorous tensor approach with the more economical scalar method is very important. A second difference between MT and CSAMT is the fundamental low-frequency limit encountered by the latter beyond which the assumption of plane-wave geometry is not met. This limit depends upon separation of source and receivers and, in often complicated ways, upon the resistivity structure hosting both (Zonge and Hughes, 1991). There has been limited computer simulation of transmitter effects with inhomogeneous structure in CSAMT (Sandberg and Hohmann, 1982; Boschetto and Hohmann, 1991) but not a detailed analysis incorporating both field data and theory.

There is an unusual opportunity to advance understanding of the CSAMT method through the comprehensive data set and analysis methods at hand. First, we have recently completed an extensive tensor CSAMT survey of the Sulphur Springs geothermal area, Valles Caldera, New Mexico (Figure 1). This survey, consisting of 45 high-quality sites acquired in continuous-profiling mode, has been funded by DOE/OBES in support of CSDP drillholes VC-2A and VC-2B (Heiken et al., 1990; Goff et al., 1992). Second, our research group has developed leading algorithms for the interpretation of inhomogeneous EM responses, both plane-wave and finite source. Derivation of model resistivity cross sections from our data set

and their correlation with structure and geochemistry are primary components of the project. However, Sulphur Springs also can serve as a natural testbed of traditional assumptions and methods of CSAMT with quantification through rigorous model analysis.

It is an additional purpose, therefore, to relate the detailed resistivity model of the Sulphur Springs area from our measurements to a general and simplified model of the caldera resistivity as a whole, and to compare this structure to that external to the caldera relatively unaffected by caldera deformation and hydrothermal alteration. Subsequently, scalar, vector and tensor CSAMT data may be contrasted over the area and discrepancies explained in relation to inhomogeneity (through the tensor elements) and EM field orientation. Controls on near-field transmitter effects can be quantified, to show whether they depend mainly on local structure, the caldera host, or a combination of both. In terms of both host and generalized caldera structure, we compare theoretical and observed electric and magnetic field geometries as a function of frequency over the survey area. Conclusions of such analyses can be verified by existing natural field MT soundings within and outside the caldera. This additional goal of examining tensor methodology in a complicated environment forms a logical complement to the geologic interpretation of resistivity in the Sulphur Springs vicinity, an interpretation well-constrained by extensive surface mapping, core-drilling, and geochemistry.

## GEOLOGICAL SETTING AND PRIOR RESISTIVITY SURVEYS OF VALLES CALDERA AND SULPHUR SPRINGS

The Valles caldera complex, centrally located in the extensive Jemez volcanic field, has been the site of groundbreaking studies of resurgent calderas by the U. S. Geological Survey (Smith and Bailey, 1968; Heiken et al., 1990). With support from the Dept. of Energy/Office of Basic Energy Sciences, Continental Scientific Drilling Program (CSDP) core holes VC-2A and VC-2B were completed in the Sulphur Springs area of the western Valles caldera (Figure 2). Their primary purposes were (a) to obtain continuous core through the intracaldera volcanic sequence and its basement rocks for reconstruction of caldera evolution, and (b) to help model the prodigious high temperature hydrothermal system of the Sulphur Springs area of the caldera (Hulen et al., 1988; Hulen and Gardner, 1989; Hulen et al., 1991; Goff et al., 1992).

### Geologic Setting of Valles Caldera and Sulphur Springs

The Valles caldera has been an active Quaternary magmatic system related to Miocene-to-present extensional deformation of the Rio Grande Rift and the Jemez lineament (Smith and Bailey, 1968; Aldrich, 1986; Heiken et al., 1990). After initial silicic volcanism some 3-3.5 Ma, eruptions around 1.45 and 1.1 Ma lead to two nearly coincident calderas, the Toledo first and then the Valles. The principal structural grain in the caldera area trends NE, paralleling the recurrent Jemez fault zone, which itself serves as the western boundary to the thickest pyroclastic stratigraphy (Nielson and Hulen, 1984). Sulphur Springs, the area of most active current hydrothermal manifestation, lies west of this fault zone and of the resurgent Redondo Dome (Figures 1 and 2).

Volcanic stratigraphy lie unconformably on downfaulted Paleozoic sedimentary rocks and Precambrian crystalline basement (Figure 3). The older sediments consist primarily of Madera Formation limestone under Yeso and Abo Fm redbeds; they total on the order of 750 m thick in the Sulphur Springs area as encountered in corehole VC-2B (Goff et al., 1992). Sedimentary thicknesses in and around the caldera may vary, however, due to differing paleo-erosional levels (Smith et al., 1970). The overlying Upper Tertiary Santa Fe arkose and variably-welded Lower Tuffs give way upward to two thick, usually densely welded tuffs comprising the Bandelier Formation, identified as the Otowi (lower) and the Tshirege (upper), with a total thickness of from 330 to 630 m in the western caldera complex (Hulen et al., 1991). Separating these thick ignimbrite units is less than 10 m of 'sandstones' (including also breccias and pyroclastic surge deposits), which thicken to several tens of meters near the hypothetical Plinian vent area of the Tshirege Tuff just north of Redondo Peak (Hulen et al., 1991). Fracture porosity is abundant in the Bandelier section in VC-2B, but relatively rare there in VC-2A (Hulen et al., 1988; Hulen and Gardner, 1989). The highest lithology in the western area includes porous caldera-fill sediments and debris flow. Present also, mainly around the margins of the Sulphur Springs area, are flows of the San Antonio Mountain ring-fracture vent (west of Sulphur Creek Fault) and of Redondo Creek Graben (in the east portions of area). A more detailed map of Sulphur Springs vicinity is given in Figure 2. Volcanic strata total less than 1 km in thickness in the western caldera complex whereas a column approaching 4 km is interpreted to lie in the deep east moat of the caldera (Heiken et al., 1990).

Hydrothermal alteration in the Sulphur Springs area has been interpreted to consist of three depth zones: illite/smectite, illite and propyllitic minerals (+- K-feldspar) (Hulen and Nielson, 1986a; Hulen and Gardner, 1989). The upper clay-rich zones are on the order of 250 - 300 m thick, extending through the caldera-fill sediments and into the only moderately-welded, highest levels of the Tshirege tuff. Illite abundance decreases dramatically at greater depths with the onset of dense welding of the tuffs, and hydrothermal propyllitization dominates below about 400 m. Alteration at depth appears broadly similar to that in the Redondo Dome area (Hulen and Nielson, 1986b), with the most important controls being the temperature gradient, fluid composition and rock permeability. The latter in turn is correlated with stratigraphy and so alteration assemblages show a near horizontal disposition. However, illite-smectite clays have been preserved in the Paleozoic clastics despite elevated temperatures, presumably due to low permeability (Hulen and Gardner, 1989). Also, the geothermal fluids responsible for alteration in the Sulphur Springs area are interpreted to be distinct to some extent from those of Redondo Creek area (Hulen and Nielson, 1986a; Goff et al., 1988). There are also local zones of intense phyllic alteration associated with major thermal fluid entries (from fractures) in the wells of both areas (Hulen and Nielson, 1986b; Hulen and Gardner, 1989).

Resistivity Determinants at Sulphur Springs

In the Sulphur Springs geothermal area, the dominant controls on bulk rock resistivity should be electrolytic conduction through rock pores and fractures and along mineral surfaces (especially clays) (Olhoeft, 1981). Electrical conductivity $\sigma_r$ (inverse of resistivity $\rho_r$ ) of rocks containing relatively conductive fluids is often described using Archie's Law, which is

$$\sigma_r = A \sigma_w \phi^m \qquad (1)$$

where A is a geometric constant, $\sigma_w$ is the pore water conductivity, $\phi$ is rock porosity, and m is the tortuousity coefficient dependent upon pore geometry. For most rocks and sediments when conduction is through intergranular pores, A = 1 and m = 2 based on empirical observation. For randomly oriented fractures, A = 2/3 and m = 1. Because m = 1 for fractures, they may be effective in reducing bulk resistivity even if they constitute a minority of total porosity.

The total dissolved solids content observed in fluids in the western Valles system lies around 0.1 N and is primarily NaCl (Hulen and Nielson, 1986b; J. B. Hulen, pers. comm., 1991). Over the temperature range 20°C to 250°C, the conductivity of such a fluid may vary from 1 to 5 S/m (resistivity from 1 to 0.2 ohm-m) (Quist and Marshall, 1968). For unconsolidated caldera-fill sediments in the upper 200 m or so of the section with a porosity on the order of 15%, a representative bulk resistivity may be around 30 ohm-m. For the welded ignimbrite section below with intergranular porosity of only a few percent, resistivities of hundreds of ohm-m may be possible. This would disregard contributions from fracture porosity. Lower resistivities may be expected again in the more porous and permeable Lower Tuffs and arkose, and the Paleozoic sedimentary rocks, while high resistivities are presumed typical of the metamorphosed and relatively impermeable Precambrian rocks.

Clay minerals can lower rock resistivities substantially by contributing exchangeable cations to the pore solution (e.g., Waxman and Smits, 1968). This effect is strongest for very dilute pore fluids. Measurements by Ward and Sill (1976) on highly altered samples from the Roosevelt Hot Springs thermal area (Ward et al., 1978) with pore fluids near 0.1 N NaCl suggested that clays might reduce resistivities of porous sediments by a factor of 2 to 4. Thus, unconsolidated caldera fill and debris flow in the Sulphur Springs area may show resistivities as low as 10 ohm-m. Below 250 - 300 m in the densely welded tuffs and especially in the propyllitic regime, the contribution of clays to reducing resistivity should be much decreased compared to within the shallowest units. Clays are likely to remain important in lowering resistivity in the Paleozoic section. Porosity and the degree and species of clay alteration logged in wells B-8 and VC-2A and VC-2B should provide some calibration of a CSAMT model for the entire survey area.

On the basis of its acid springs and fumaroles, and of steam entries and sub-hydrostatic pressures in wells, Sulphur Springs has been interpreted as the surface expression of a small, vapor-dominated geothermal system (Goff et al., 1985). Vapor-dominated systems are important to the geothermal industry because they may yield dry steam, which is the most economically desireable geothermal resource. A boiling interface to a liquid-dominated regime below is believed to lie at a depth of around 500 m beneath Sulphur Springs (op. cit.). The electrical conductivity of pure, dry steam is very small, with the conduction of steam-filled rock being due largely to condensation and surface conduction along pore walls, a mechanism not yet adequately studied (Olhoeft, 1981). Zohdy et.al., (1973) interpreted a high-resistivity steam zone in Yellowstone using dipole-dipole resistivity. Estimating resistivity of the vapor zone at Sulphur Springs has been one of the primary purposes of our CSAMT survey.

Prior Electrical Resistivity Surveys at Valles Caldera

Direct-current (dc) resistivity soundings for assessment of hot dry rock geothermal resources have been described by Jiracek et al., (1975). These included roving bipole-dipole reconnaissance, shallow Schlumberger soundings and deep dipole-dipole soundings concentrated in the Fenton Hill area (Figure 1). Layered sounding models, constrained by drilling logs, showed a thin (100 m) section of volcanics of variable resistivity over a thick section (633 m, similar to VC-2B) of Paleozoic sediments, with both clastics and carbonates showing low resistivity around 15 ohm-m. Crystalline Precambrian basement below 733 m exhibited high resistivity of hundreds to thousands of ohm-m. A 300 ohm-m zone 100 m thick near the upper surface of the basement corresponded to a highly fractured zone with considerable water content (Jiracek et al., 1975).

An extensive review of the upper crustal geology and geophysics of Valles caldera has been given by Wilt and vonder Haar (1986). An averaged resistivity log of the volcanic section near the northern end of Redondo Creek graben shows low resistivities (2-10 ohm-m) in porous and altered sediments of the upper 200 m, but a generally resistive (100-500 ohm-m) Bandelier Tuff section below over 1 km thick. Low resistivities (10-70 ohm-m) are seen again in the more porous Lower Tuffs and pre-caldera volcanics containing hot saline reservoir fluids (Wilt and vonder Haar, 1986). Resistivity sections derived using telluric and magnetotelluric (MT) profiling showed a lower resistivity volume at a depth near 1 km roughly coincident with

the Redondo Creek graben reservoir zone, and a low resistivity section of thick sediments in the Valle San Antonio moat area to the north. Low resistivities at depths from 1 to 3 km were interpreted also below a profile from the graben west to Sulphur Creek fault approximately coincident with our CSAMT line N2 (Figure 2). The MT modeling produced generally high resistivity values for the Bandelier Tuff as well (>100 ohm-m) over both MT profiles analysed. However, we expect some variance between this latter model cross section and those resulting from our data and analysis, stemming primarily from our contiguous data coverage and the multidimensional modeling approach we will take.

Thirty-one MT soundings for geothermal assessment in Valles caldera were taken by Unocal Geothermal Co. in the early 1980's (Crecraft et al., 1988; Figure 1). The cross-spectra for these soundings have been released to us and processing of these to reconstruct the impedance data is a goal of the near future. These data will be valuable in constructing an overall resistivity model at upper crustal levels at Valles caldera for model control of our Sulphur Springs data set as well as allowing a thorough analysis of controlled-source effects in the CSAMT method. To these ends also, MT soundings taken by San Diego State University as part of their Summer of Applied Geophysical Experience (SAGE) program (Jiracek et al., 1991) both within and outside the caldera will be very useful. Some of this latter data will be compared to our own shortly.

## TENSOR CSAMT DATA FROM THE SULPHUR SPRINGS AREA

This section discusses the experimental approach in carrying out a tensor CSAMT survey in the Sulphur Springs area. After a brief review of basic methodology for tensor acquisition, I describe the quality and characteristics of our data set, and some qualitative features considered relevant to the geology of the western caldera.

### CSAMT Methodology

Schematics of the field layout for the general tensor CSAMT survey mode are given in Figure 4 (Zonge and Hughes, 1991). For the simplified scalar setup, the broadside deployment is very popular. Here, single electric and magnetic field sensors (i.e., $E_{y1}$ dipole and $H_{x1}$ coil) at a receiver site measure fields from a single current bipole (Tx-1) displaced from but parallel to the electric receiver. Scalar impedances, apparent resistivities, and impedance phases are obtained from simple field ratios. The broadside source displacement from the receiver need not be quite as large as an end-on source displacement (three skin depths in the most representative medium for the former versus five skin depths for the latter; Sandberg and Hohmann, 1982; Zonge and Hughes, 1991) and typically yields twice the signal strength for a given displacement as the end-on deployment (op. cit.). Often, a contiguous array of electric field bipoles is oriented across presumed geologic strike with a magnetic field sensor placed intermittently along the profile. This layout has been applied widely to structural mapping in precious metal and hydrocarbon environments because the electric field thus measured is more sensitive to fault displacements of conductive alluvium and the 2-D assumption is relatively valid for this geometry (the transverse magnetic or TM mode; Wannamaker et al., 1984: Vozoff, 1991). As profiling data is acquired, the source bipole would 'leap-frog' along to ensure good signal coupling with the receiver sensors. Good signal typically is available in a 90° wedge subtending broadside from the source, outside of which the fields are too oblique to the measurement axes to obtain reliable data (Sandberg and Hohmann, 1982; Zonge and Hughes, 1991).

For the tensor CSAMT method, five EM field components ($E_x$,$E_y$,$H_x$,$H_y$,$H_z$) are measured for two independent polarizations of source current bipole (i.e., ten fields in all at each site). Plane-wave impedances, apparent resistivities and impedance phases are not defined by simple field ratios as in the scalar approach, but instead by solution of a series of 2 x 2 matrix equations determined from the fields due to the two sources. The procedure in fact is identical to that used in computer simulation of tensor impedances over multidimensional models (e.g., Wannamaker et al., 1984). For example, the solutions for the off-diagonal impedance elements in terms of the measured fields are

$$Z_{xy} = \frac{E_x^2 H_x^1 - E_x^1 H_x^2}{H_x^1 H_y^2 - H_x^2 H_y^1} \qquad (2)$$

and

$$Z_{yx} = \frac{E_y^2 H_y^1 - E_y^1 H_y^2}{H_x^1 H_y^2 - H_x^2 H_y^1} \qquad (3)$$

where superscripts 1 and 2 refer to the source bipole number. As is the case for numerical simulation, it is not necessary that all field components be strongly excited for both source polarizations but instead that each component be excited by at least one source. It is obvious that tensor data is considerably more time-consuming to acquire than scalar data, but the tensor response has the great advantage that it is unambiguous regardless of the dimensionality of the field environment.

A collection mode intermediate between scalar and tensor is the vector CSAMT setup (Zonge and Hughes, 1991). Here, all four horizontal fields are also measured (plus $H_z$ if desired), but only one source bipole is energized. This allows construction of the total field vectors (E and H) at the receiver regardless of its orientation. Vector measurements thus can provide two orthogonal scalar impedances, or else one impedance based on the total (i.e., best-coupled) fields.

Scalar and tensor CSAMT quantities can be contrasted by examining either row of the 2 x 2 tensor impedance. For $E_y$ it is

$$E_y = Z_{yx}H_x + Z_{yy}H_y \qquad (4)$$

When normalized by $H_x$ we have

$$\frac{E_y}{H_x} = Z_{yx} + Z_{yy}\frac{H_y}{H_x} \qquad (5)$$

Note that the ratio on the left-hand side is just the scalar yx impedance. It differs from the true tensor impedance $Z_{yx}$ by the far right-hand term: the product of tensor element $Z_{yy}$ and the ratio $H_y/H_x$. If $Z_{yy}$ is essentially zero, or negligible $H_y$ is induced by the source bipole, the scalar and tensor quantities will agree well. As $Z_{yy}$ and $H_y/H_x$ become significant, however, discrepancies can be expected. In fact, for receiver sensors poorly coupled to the source field for the ,e.g., $E_y$-$H_x$ scalar measurement, $H_y/H_x$ may become much greater than one and substantial disagreement between scalar and tensor quantities ensue even though the multidimensionality (i.e., $Z_{yy}$) may be quite small. This effect should be most likely as one approaches the boundaries of the wedge-like zones of good field coupling noted previously. It may be responsible in large part for apparent transmitter overprint effects (Zonge and Hughes, 1991) such as commonly seen at joins between E-field spreads measured with different broadside transmitters. Examples will be presented from the Sulphur Springs area as well.

A different but equally important topic effecting both scalar and tensor CSAMT data is the plane-wave assumption toward low frequencies. For sources and receivers on a uniform half-space, separations of three to five skin depths at the lowest frequency of interest produce departures from true plane-wave responses of about 5% or less (Goldstein and Strangway, 1975; Sandberg and Hohmann, 1982). For layered earths, the departures can sometimes be very sensitive functions of the layering and source-receiver separations (Figure 5; Zonge and Hughes, 1991). Limited modeling of 3-D structure below CSAMT transmitters indicates that conductive inhomogeneity there can prolong the far-field assumption to somewhat lower frequencies relative to a half-space, while resistive inhomogeneity has an opposite effect

(Boschetto and Hohmann, 1991). Attempts to correct for the transition to the near-field are based upon 1-D earth models (Zonge and Hughes, 1991). Perhaps the most rigorous technique within the 1-D framework is to invert each sounding using the true finite source over a layered earth, and then compute the plane-wave response of the resultant 1-D model. This would assume that inhomogeneous effects are limited in the sense that the effects would be similar for both plane-wave and finite source responses. We have not yet seen a study comparing near-field correction methods using coincident CSAMT and natural-field MT soundings.

Tensor CSAMT Data Acquisition Procedure at Sulphur Springs

Transmitter placement in CSAMT surveys involves a compromise between two competing issues. On the one hand, to obtain planar EM waves, the transmitter-receiver separation should be as great as possible; a doubling of this separation effects a fourfold decrease in the frequency at which near-field effects first appear (Goldstein and Strangway, 1975; Zonge and Hughes, 1991). On the other, however, signal strength varies as the inverse cube of distance (op. cit.) effecting an upper limit on separation determined by telluric and other noise sources. At Valles caldera, our transmitter was a Zonge Engineering and Research Organization model GGT-30 placed approximately 13 km (8 miles) south of the VC-2B wellhead (Figure 1). As demonstrated shortly, this position appeared to give good signal strength over the Sulphur Springs area while allowing some near-field effect at 1 and 2 Hz, which is at the bottom of our measurement range.

The two independent transmitter bipoles (TX1 and TX2 in Figure 1) for tensor measurements were oriented about N28°W and N45°E and were just over 2 km in length each. While not quite 90° apart, these orientations gave source fields over the receiver sites which were substantially independent in polarization and provided well-resolved tensor elements. Contact with the ground was made by augering five holes about 2-1/2 feet deep and about 15 feet apart in a star pattern at the end of each bipole (20 holes in all). Brass rods and braided cabling provided contact with the earth in each hole, which was filled with unconsolidated soil and ice melt compound and saturated with saline water at least every other day. The 15 foot separation between contact points ensured a nearly parallel circuit of ground resistances and gave a DC impedance of about 40 ohms between endpoints of each transmitter bipole. Consequently, current loads of 20 amps typically were possible except at the highest frequencies (above 1 kHz) where the inductance of the wire became important (Zonge and Hughes, 1991). This inductance reduced transmitter currents to as small as 5 amps at 4.1 kHz and prevented usable data at 8.2 kHz.

The soundings in the Sulphur Springs area were arranged in four profiles to cross major structural features (Figure 2). At each receiver, two orthogonal electric and three orthogonal magnetic field components were acquired in accordance with tensor principles as described with Figure 4. The electric bipoles parallel to each profile were deployed contiguously to ensure against spatial aliasing of the impedance response corresponding to current flow across structural trends (EMAP mode; Bostick, 1986; Torres-Verdin and Bostick, 1991). All bipoles normal to each profile and most bipoles along each profile were nominally 250 m in length. Some bipoles along the profiles near their ends were 500 m long to extend data coverage efficiently away from coreholes VC-2A and VC-2B. The x-axis is assigned to the northeast

direction while the y-axis is southeast. The frequency range of acquisition was 4096 Hz down to 1 Hz for the central line N1, but only down to 4 Hz for most of the other lines. Data to 1 Hz was taken at selected sites on the other lines for control. We found that fully one-third of the recording time at a site was spent taking the 1 and 2 Hz results. Fields were recorded on a Zonge Engineering Org. model GDP-16 receiver with data blocks downloaded to an IBM-compatible PC at the end of each working day for final processing. Magnetic field sensors were obtained from Electromagnetic Instruments Inc.: model BF-4 with custom amplifiers capable of acquiring data to 10 kHz.

Data quality was established by repeatability of measurements. Typically, five readings at each frequency were taken for each source bipole. Tensor impedance elements were computed for each pair of readings for the two source bipoles using equations (2) and (3), and analogues for the on-diagonal elements. Following removal of occasional outliers, means and error intervals were obtained for the tensor log apparent resistivities and linear phases over each group of readings (Bevington, 1969) in accord with the assumption of Gaussian noise on the output (electric) fields (Gamble et al., 1979; Stodt, 1983). Results were obtained similarly for real and imaginary components of the tensor tipper elements.

Observed Tensor CSAMT Results in the Sulphur Springs Area

An example tensor apparent resistivity sounding in the Sulphur Springs area is given in Figure 6. I postpone presentation of data from outside the caldera until discussion of resistivity models. The site in Figure 6 is immediately east of corehole VC-2B and a natural field MT sounding taken only several tens of meters to the west of it by G. R. Jiracek is included for comparison. The CSAMT data quality appears very good here and this quality is typical of the majority of sites in our survey. Also, the agreement between the controlled-source and natural field data is very good over almost all the period range of overlap indicating that we are free of calibration problems and that far-field results are generally being obtained. The disagreement between controlled and natural source data is substantially apparent at 1 and 2 Hz, especially the impedance phase. Our phases drop to very small values while the apparent resistivities exhibit the transmitter notch behavior exemplified in Figure 4b indicative of a conductive layer over a resistive basement. Apparent resistivities of 10 ohm-m or less are characteristic as the near-field behavior is approached over most sites in the Sulphur Springs survey. However, at 2 Hz for a half-space of 10 ohm-m, our transmitter would be more than 10 skin depths removed. It suggests that half-space calculations based on apparent resistivity in the vicinity of the receiver array may not be a sufficient determining factor in the near-field response. This point will be reconsidered when we show data from outside the caldera.

For the central, longest line N1 of Figure 2, our tensor data are summarized in the form of pseudosections, wherein site position serves as abscissa and log period serves as ordinate for contour plots of log apparent resistivity, impedance phase, and complex tipper elements (Figures 7 and 8). The lowest apparent resistivities for both the nominal TE (xy-mode) and TM (yx-mode) data occur between the Sulphur Creek and Freelove Canyon faults with shortest-period values just over 10 ohm-m falling to just under 10 ohm-m by about 0.03 s (Figure 7). A mild apparent resistivity maximum near 0.1 Hz suggests a resistive units a few hundred meters in depth, with a decrease in resistivity below (apparent in Figure 6 also),

although detailed modeling is necessary. This feature is more pronounced at the next two sites to the west and along strike to the south along profile S1, but is not obvious on line N2. East of Freelove Canyon Fault, substantially higher resistivities are evident at periods less than 0.01 s suggesting relatively unaltered surficial volcanics perhaps including Redondo Creek flows. A substantial thickness of outcropping resistive volcanics is apparent west of Sulphur Creek fault over flows from San Antonio Mountain dome and related ring-fracture vents. At periods greater than 0.25 s ($f < 4$ Hz), the transmitter notch behavior exemplified in Figure 6 can be seen for all stations west of Freelove Canyon fault, but not to the east (Figure 7). This implies a major structural boundary; at the surface, the change corresponds to the Freelove Canyon fault, a major normal fault with downdrop to the east.

The vertical magnetic field responses over the survey area are not highly anomalous (Figure 9). For periods under 0.01 s, the values appear to correspond with local topographic slope orientations (e.g., Wannamaker et al., 1986). Between Sulphur Creek and Freelove Canyon faults, a transmitter near-field effect appears to develop for periods greater than 0.25 s. Anomalies reaching 0.15 near Sulphur Creek and Freelove Canyon faults may be related to subsurface structure, but the topographic relief along the profile must be considered in any model. The lack of an appreciable vertical field response due to subsurface structure may be valuable information in itself as it relates to limited strike extent of the structure (e.g., Wannamaker et al., 1991).

## RESISTIVITY MODELS FROM OBSERVED DATA

Controlled-source data were acquired both within and outside Valles Caldera because it is believed that the resistivity structure of the two areas may differ substantially due to caldera processes. The primary purpose of the survey has been derivation of a detailed resistivity model of the Sulphur Springs areas and its correlation with the hydrothermal system. However, from the standpoint of EM interpretation, it is important to consider whether the CSAMT data around Sulphur Springs depends primarily upon local structure or is influenced strongly by resistivity of the host rocks to the caldera.

### Resistivity Structure Outside Valles Caldera

A tensor CSAMT sounding taken outside Valles Caldera to the west on Schoolhouse Mesa (site SM, Figure 1) is shown in Figure 10 and merged with MT data taken nearby on Lake Mesa (site LM) by G. R. Jiracek. Our sounding overlies a few hundred meters of Bandelier Tuff, underlain in turn by the pre-caldera volcanic and Paleozoic sedimentary section, and the Precambrian basement (Smith et al., 1970). The stratigraphy beneath the CSAMT and MT sites is presumed to be essentially equivalent except perhaps at the highest levels due to differing erosion. The MT apparent resistivities required a very small static shift (0.05 log units) to join the CSAMT results.

To begin, the tensor CSAMT results were inverted using a layered-earth, Marquardt-type damped least-squares algorithm similar in construction to the plane-wave code of Petrick et al. (1977). However, the CSAMT inversion algorithm here rigorously considers the finite source effects, and includes transmitter and receiver bipole lengths and orientations and the tensor nature of the data in the calculations. From this inversion, the parameters of the upper four layers of the five-layer earth defined in Figure 10 were obtained with resolution within a few to ten log percent and a reduced chi-squared of about five. Subsequently, the MT data were inverted with this upper layering constrained to obtain the depth and resistivity of the regional deep conductor (25 ohm-m at 10.5 km nominally). The inversion parameters, together with the regional geological mapping (Smith et al., 1970) and drill logs from the Fenton Hill site (Jiracek et al., 1975), imply over 200 m of resistive Bandelier Tuff underlain by a similar thickness of low resistivity (10 ohm-m) Paleozoic sedimentary rocks. The basement rocks are resistive, although not highly so; values in the thousands of ohm-m produce low-frequency CSAMT responses which climb to unacceptably high values (not shown).

The reduced chi-square error in the CSAMT inversion could be lessened somewhat (to about 3.5) by allowing a low-resistivity layer at a depth around 2 km, but this clearly disagrees with the MT data. The minor lack of fit in the CSAMT results at frequencies of 4 Hz and below (especially the phase) therefore is attributed to inhomogeneity which may exist anywhere in a poorly-defined region encompassing the receiver and the transmitter. An attempt was also made to invert the CSAMT data with the pronounced low-resistivity layer at a depth of about 235 m constrained to have a thickness of 635 m, about that reported from drill-logs at Fenton Hill (Jiracek et al., 1975). However, this worsens the fit somewhat (reduced chi-squared over eleven, dotted curve in Figure 10). The discrepancy between this data and the drill logs cannot be explained definitively at present, but may represent differing erosional levels in the

Paleozoic sediments when the volcanic sequence was laid down.

Construction of Two-Dimensional Resistivity Models

Detailed resistivity sections from the CSAMT data taken along the four profiles shown in Figure 2 are being derived through 2-D finite element forward modeling and parameterized inversion of the plane-wave regime data, using layered earth inversion models as starting guesses. In this procedure, the data set corresponding to current flow across presumed geologic strike (N45°E), the so-called transverse magnetic (TM) mode, is emphasized because it is relatively immune to structural variations along strike (Wannamaker et al., 1984). The 2-D forward modeling uses the algorithm described by Wannamaker et al., (1986, 1987). The parameterized inversion code based on this forward program essentially follows the procedure of Oristaglio and Worthington (1980). The inversion, using Marquardt's method and which did not attempt to damp model roughness, was carried out following the forward modeling and was intended to tighten the fit by improving estimates of the resistivity primarily in the upper 300 m. Topographic variations along the profiles are substantial and are included in the 2-D modeling. The fit of the TM mode response of this model is exemplified in the sounding plots of Figures 6 and 13. Resolution in the cross sections can be assessed by perturbing key features and assessing the change in computed response relative to the data (hypothesis testing). Depth extent of the cross sections can be increased somewhat by limited incorporation of the natural-field MT data taken near well VC-2B. At present, modeling has been completed only on the longest, central profile N1 straddling corehole VC-2B, but comparisons with the data of profile S1 running beside well VC-2A will be made. The lithologic logs of these two coreholes are very valuable in relating resistivity structure to geology. Modeling was carried out on an IBM-compatible 80486 PC with processor speed of 66 MHz.

The preferred model of the central line N1 is presented in Figure 11. Details of the finite element mesh geometry have been preserved but resistivity values have been grouped into half-decade intervals for simplicity. East of Sulphur Creek fault (station 5 approximately), the upper 200 m of the section is of relatively low resistivity (5 - 30 ohm-m) and corresponds to unconsolidated landslide and debris flows (formerly pyroclastic). At the easternmost end of the profile on Redondo Border, there may be several tens of meters of resistive rhyolite flow capping the section which is related to the resurgent dome. In the depth interval 200 to 750 m east of Sulphur Creek fault, as constrained from the VC-2B well log, the substantially welded Bandelier Tuff sequence exhibits relatively high resistivities (200 - 300 ohm-m), similar in values to those reported for electric logs from the Redondo Graben area and to those interpreted from the CSAMT data exterior to the caldera. Below the Bandelier Tuff, the Paleozoic sedimentary sequence was fixed to be 750 m thick in accordance with the VC-2B log. Thus constrained, its interpreted resistivity appears somewhat lower (about 5 - 8 ohm-m) than such sediments below Schoolhouse Mesa, perhaps related to the preserved clay alteration described earlier. This conclusion is based primarily on the natural field MT data at VC-2B and it is difficult to constrain the layer conductance precisely along the rest of the profile just from the plane-wave regime data. Toward the east end of the profile, evidence for this sedimentary layer disappears, in apparent keeping with structural interpretations of a substantial downdrop of the section to the east across the Freelove Canyon normal fault. The presence of this

sequence at the easternmost end of the cross section is based on drilling results from the Redondo Graben area (Goff et al., 1992). At depths beyond about 1500 m below the surface, MT data near well VC-2B indicate resistive basement corresponding to the crystalline Precambrian.

No particularly high resistivities possibly corresponding to a vapor zone in the upper 500 m near VC-2B, as implied from acid-sulphate alteration and subhydrostatic well pressures (Goff et al., 1992), are evident in the CSAMT data. However, the Sulphur Creek fault itself appears to be a locus of substantial change in structural relief; upthrow of stratigraphy and basement to its west appears to be about 400 - 500 m. At the surface here, a somewhat eroded Bandelier sequence with a thin veneer of ring-fracture dome rhyolite continues westward to the limit of the profile essentially at the caldera ring fracture. No further structural relief is detected west of Sulphur Creek fault. This is at variance with published geologic cross sections based on sparse drilling data and surface mapping, which show a nearly continuous distribution of normal faulting but which are poorly constrained in this area.

## ANALYSIS OF THE CSAMT METHOD AT VALLES CALDERA

Given the current state of numerical simulation technology, the resistivity structure in the Sulphur Springs area has been derived almost exclusively from the component of CSAMT data which lies in the plane-wave regime. With this model structure, however, and with the availability of tensor CSAMT and MT data both inside and outside Valles Caldera, the Sulphur Springs data set also can serve in the analysis of CSAMT methodology with regard to non plane-wave effects, source field orientations, and scalar versus tensor quantities. The finite source analysis in the end may also augment our structural understanding.

### CSAMT Near-Field Behavior

To start, I consider CSAMT and MT data acquired outside the caldera. The high-quality tensor CSAMT sounding at Schoolhouse Mesa (Figure 10) implies a high degree of resistivity isotropy in its vicinity, and this is supported by the nearby MT site. Comparison of CSAMT and MT responses calculated from the one-dimensional inversion model indicate that non plane-wave effects enter the CSAMT data at 8 Hz and lower frequencies. At 8 Hz, the data are beginning to sense the crystalline basement at a depth just under 500 m. This is only about 1/20th of the transmitter-receiver separation (about 10 km) and is much more pessimistic than traditional assumptions about available depth of exploration in the plane-wave regime (usually 1/5th the separation or more). This is interpreted to result from transmitter EM fields entering the basement in the vicinity of the transmitter and propagating to the receiver with relatively little attenuation.

Furthermore, comparison of observed electric (E) and magnetic (H) fields at this site with those computed from the layered resistivity model derived from 1-D inversion of the apparent resistivity and impedance phase can provide information about structure below the transmitter site (Figure 12). Small-scale (on the order of 1 km or less), non 1-D structure below the transmitter may influence details of the return current flow from the source bipole contacts and cause equal log shifts in E and H data relative to the computed fields which are constant versus frequency. Small such shifts (about 0.1 log unit) are observed in one mode of the measured fields, but not discernable in the other, down to a frequency of about 8 Hz. This behavior indicates that such small-scale structure does not lead to transmitter overprint effects in the impedance data at the receiver but instead acts as an equivalent far-field source. However, scales of inhomogeneity much larger than this are evident in the raw fields. Below 8 Hz, the observed E and H fields fall substantially below those computed from the layered model and suggest structure of several kilometers scale around the transmitter may be conductive relative to the receiver.

In the Sulphur Springs area, coincident CSAMT and MT data near well VC-2B indicate slight non plane-wave effects in the former data may be occuring at 4 Hz, but are much more obvious at 2 Hz and below. In fact, apparent resistivities around VC-2B lie near or below 10 ohm-m over almost all the frequency range so that the appearance of any near-field effect would not be expected based on a straightforward half-space analysis. It is probable that the resistive crystalline basement is important here as it was for the data exterior to the caldera. In order to pursue the structure controlling non plane-wave effects in the Sulphur Springs area,

site 10 of profile N1 is considered (Figure 13). The position of this site in the 2-D model and the isotropy of the tensor response suggest that a 1-D analysis may be fruitful. Otherwise, the data is very similar to that at the VC-2B well site including the apparent near-field effects. A 1-D tensor CSAMT inversion of these data was performed with the thicknesses of the Bandelier and Paleozoic sections constrained to be those of the 2-D model. The inversion provided a close fit to the data with, in particular, Paleozoic sedimentary resistivity close to that derived in the 2-D model around VC-2B. Shown also is the 1-D CSAMT response computed at this location but using the resistivity and thickness of the Paleozoic sediments derived at Schoolhouse Mesa outside the caldera. The conductance (thickness divided by resistivity) of the sediments at Schoolhouse Mesa is only about one-quarter that derived at site 10. The response using the Schoolhouse Mesa model shows a non plane-wave effect occuring at a much higher frequency which is not in accord with the data. This examination suggests that the resistivity section from the resistive Bandelier Tuff downward interpreted in the Sulphur Springs area is more representative for the entire western caldera and the region outside the caldera to the west than is this portion of the section around Schoolhouse Mesa analysed previously. This is an example where full controlled source interpretation can augment structural interpretation over just the plane-wave regime results.

A yet clearer picture of the effective regional structure governing the controlled-source EM response emerges if one examines the raw electric and magnetic fields at site 10 (Figure 14). Plotted with the field data are the calculated responses using the 1-D model derived just previously from the CSAMT inversion at site 10 (long dashes) and the 1-D model derived from the inversion of the data at Schoolhouse Mesa (short dashes). Only the responses due to transmitter bipole 1 are shown because those from bipole 2 appear identical to within 0.02 log units. Consider first the magnetic fields (lower panel of Figure 14). The local resistivity model used in a 1-D calculation gives magnetic fields which are clearly much smaller than the observations especially at the higher frequencies, although agreement in better at the lower frequencies. On the other hand, the layering derived at Schoolhouse Mesa provides good agreement with the data at all but the lower frequencies, where the calculations appear too large. An equivalent layered sequence which gives reasonably good agreement with the H-field observations over all frequencies can be defined simply by inserting Paleozoic layering whose resistivity and thickness are those deduced below site 10 into the model sequence derived at Schoolhouse Mesa (solid curves of Figure 14). Note that none of the prior layered sequences agrees with the electric field amplitudes in the upper panel of Figure 14. This is because the E-field strength is influenced by both the regional and the local structure. This study should make clear the ineffectiveness of inversion of observed electric or magnetic fields to derive local resistivity structure; apparent resistivity and impedance phase which are independent of source field strength are preferable for that. However, behavior of the fields, especially the magnetic, can be very useful for understanding the regional scale resistivity which controls the non plane-wave effects and the field amplitudes.

Controlled-Source Field Geometries at Sulphur Springs

Decisions regarding transmitter orientation and placement to achieve good source field coupling at receiver sites are typically made on the basis of half-space calculations of EM field

geometries (Goldstein and Strangway, 1975; Sandberg and Hohmann, 1982; Zonge and Hughes, 1991). When the field area departs negligibly from a half-space, agreement between observed and theoretical field responses is good (Goldstein and Strangway, 1975). In arbitrary structural environments, such agreement should not be presumed, especially for scalar measurements. As a test of the variability of source geometries in possibly complex areas, we process and examine the raw electric and magnetic fields taken in our survey for comparison to theoretical computations. Field quantities are presented as polarization ellipses, as we have already utilized in theoretical studies (e.g., Wannamaker et al., 1984). Data statistics of the ellipse parameters are calculated through repeat measurements.

Observed electric (E) and magnetic (H) field ellipse axes with error intervals at 128 Hz are plotted in Figure 15 for both transmitter bipoles. The ellipse orientations for the two source bipoles are clearly quite independent allowing well-resolved tensor elements. Calculated E- and H-field ellipse axes using a 1-D model based on the effective regional resistivity host derived from the data of site 10 of line N1 (recall previous discussion of near-field effects) follow in Figure 16 for comparison. The small, static transmitter effect of about 0.1 log units has been removed from the computations. The agreement between observed and computed H-field ellipse axes is close, apart from minor site-to-site variations in the observed data due presumably to local heterogeneity. This suggests that the incident field strength and orientation (of interest for survey design purposes) has not been seriously distorted by any large-scale inhomogeneity. The observed electric (E) fields are much more strongly affected by geology, with relatively small values over the geothermal system near and east of Sulphur Creek and large values over the volcanic sections toward the east and west ends of the survey area, compared to the calculated E-fields. Numerous and sometimes strong, site-to-site variations due to small-scale structure are evident also. At the lowest frequencies (1 and 2 Hz), the observed fields become elliptically polarized (e.g., Figure 17). However, the computed fields do not exhibit this effect and I do not have a firm explanation at this time.

Static Versus Tensor CSAMT Quantities

As discussed with equations (4) and (5), discrepancies between scalar and tensor CSAMT quantities may arise due both to inhomogeneity and to oblique orientation of the source fields. Examples of such differences appear in Figure 18 for two sites on line S1. Site 19 is the fourth from the east end of the line while site 24 is at the far west end. Here are plotted $\rho_{xy}$ and $\rho_{yx}$ in separate panels for comparison with the corresponding scalar quantities resulting from the two transmitter bipoles. At site 19, the scalar results straddle the tensor values and bracket a range from about 0.3 - 0.5 log units. The two tensor curves are anisotropic by about 0.15 - 0.2 log units. The total magnetic field here due to bipole 1 lies about 60° counterclockwise (ccw) from the assumed N45°E strike while that due to bipole 2 lies about 70° clockwise (cw) from strike. That both magnetic fields have stronger y than x components may explain the greater discrepancy exhibited between the yx scalar and tensor results in light of equation (5). The on-diagonal impedance magnitudes are typically about 30% of the off-diagonal elements.

At site 24 (Figure 18), the scalar $\rho_{xy}$ due to source 1 is essentially coincident with the tensor $\rho_{xy}$, while the scalar $\rho_{yx}$ due to source 2 is essentially coincident with the tensor $\rho_{yx}$.

The other scalar quantities, however, differ by 0.3 - 0.5 log units. Here, the total magnetic field due to bipole 1 lies about 60° ccw from the assumed N45°E strike while that due to bipole 2 lies about 20° cw from strike. In this case, since each bipole's field is close to one of the coordinate directions, the tensor-scalar differences are small for the well-coupled components. This suggests that the vector CSAMT measurement discussed in an early section, which measures all fields at a receiver but utilizes only one source bipole, may be sufficient in nearly isotropic areas for resolving a stable response. At site 24, the tensor apparent resistivities $\rho_{xy}$ and $\rho_{yx}$ are isotropic to within 0.05 log units. The on-diagonal impedance magnitudes are typically about 20% of the off-diagonal elements.

The examples of differing tensor versus scalar apparent resistivities in Figure 18 were found without much searching and so it is presumed that the effect is common in the Sulphur Springs data set. A task for the near future is to compare scalar and tensor results at all sites in the survey area to characterize completely the degree to which this occurs. Initially, simple histograms of the difference between scalar and tensor log $\rho_a$ versus frequency of occurence should be useful. The larger discrepancies need to be correlated with the amount of heterogeneity present (as quantified by the on-diagonal impedance amplitudes) and to the field azimuths relative to the measurement axes. Thus, analysing the adequacy of scalar results and the orientations of EM fields over the survey area discussed previously are closely tied together. We also wish to compare the vector mode data, which can be constructed from our field results, with the tensor impedance values rotated coincident with the total field azimuths. The data shown in Figure 18 suggested that the vector mode quantities, which are still much more economical to acquire than full tensor data, may agree with the tensor results more closely in general than do the scalar quantities.

## CONCLUSIONS

Use of crossed, electric bipole current transmitters can be an effective method of obtaining high-quality tensor CSAMT data in inhomogeneous environments. Contiguous electric receiver bipoles mitigate against undersampling of the response across presumed strike. Numerous structural details in the western portion of Valles Caldera were revealed through two-dimensional modeling of the central data profile in concert with independent constraints from surface mapping and corelogs from well VC-2B. Low resistivity, unconsolidated debris flows cover much of the area, but the CSAMT data indicate that the Bandelier Tuff remains resistive below the Sulphur Springs thermal area and is of similar resistivity properties to tuff studied in the Redondo Graben area and outside the caldera. There is a substantial thickness of low resistivity below the Bandelier Tuff, primarily corresponding to Paleozoic sedimentary rocks, and which in itself does not represent a hydrothermal reservoir. The conductance of the Paleozoic section within the western caldera appears to be very much greater than that interpreted from limited data taken to the west on Schoolhouse Mesa. At depths beyond about 1500 m below the surface, MT data near well VC-2B imply resistive basement corresponding to the crystalline Precambrian. No particularly high resistivities possibly corresponding to a vapor zone in the upper 500 m near VC-2B are evident in the CSAMT data. However, the Sulphur Creek fault itself appears to be a locus of substantial change in structural relief; upthrow of stratigraphy and basement to its west appears to be about 400 - 500 m. Depth of exploration of the CSAMT data in the plane-wave regime was about 750 m; having even limited natural field MT data can extend this depth effectively.

Availability of CSAMT and MT data both inside and outside the caldera allowed some interesting analyses of the CSAMT method to be undertaken. Implied exploration depths within the plane-wave regime in this study were considerably more pessimistic than those usually offered based on half-space calculation. This is presumed to result from existence of resistive crystalline basement below the survey area allowing propagation of non-planar EM fields for great distances with little attenuation. Inhomogeneity below the transmitter did not lead to overprint effects in the impedance data at the receivers at least in the plane-wave regime. Near-field effects around Sulphur Springs suggest that the conductance of the Paleozoic sediments deduced for the western caldera is approximately representative of that over most of the region encompassing the transmitter and the receivers. However, the magnetic fields suggests that near-surface resistive layering, similar in properties to the Bandelier Tuff section, controls field amplitudes in the upper frequency range. For the magnetic fields especially, agreement between observed and computed ellipse axes is quite close over the entire survey area, suggesting that incident field strength and orientation (desireable knowledge for survey design purposes) was not substantially distorted by inhomogeneity. It may be possible to define an effective regional host using just the magnetic field, thereby allowing correction for near-field effects in the CSAMT data. When heterogeneity of any scale is important, significant departures between scalar and vector CSAMT data can be expected, and are observed in this survey. The effects are exacerbated when the source field is poorly coupled to the sensors, and so should be much reduced for vector CSAMT measurements.

## REFERENCES


Aldrich, M. J., Jr., Tectonics of the Jemez Lineament in the Jemez Mountains and Rio Grande Rift, J. Geophys. Res., 91, 1753-1762, 1986.

Bartel, L. C., and R. D. Jacobson, Results of a controlled-source audiofrequency magnetotelluric survey at the Puhimau thermal area, Kilauea Volcano, Hawaii, Geophysics, 52, 665-677, 1987.

Bevington, P. R., Data reduction and error analysis for the physical sciences, McGraw-Hill Book Co., New York, 336 pp., 1969.

Boschetto, N. B., and G. W. Hohmann, Controlled-source audiofrequency magnetotelluric responses of three-dimensional bodies, Geophysics, 56, 255-264, 1991.

Bostick, F. X., Jr., Electromagnetic array profiling (EMAP), expanded abstract, Soc. Explor. Geophys. 56th Ann. Mtg., Houston, Tex., 1986.

Corbett, J. D., Overview of geophysical methods applied to precious metal exploration in Nevada, in Geology and ore deposits of the Great Basin, ed. by G. L. Raines, R. E. Lisle, R. W. Schafer, and W. H. Wilkinson, Geological Society of Nevada, vol. II, 1237-1251, 1991.

Crecraft, H., G. Nordquist, B. M. Smith, and R. J. Varga, Evidence for geothermal upflow within the eastern half of the Valles caldera, northern New Mexico, EOS Trans., AGU, 69, 1481, 1988.

deGroot-Hedlin, C., and S. C. Constable, Occam's inversion to generate smooth, two-dimensional models from magnetotelluric data, Geophysics, 55, 1613-1624, 1990.

Gamble, T. D., W. M. Goubau, and J. Clarke, Error analysis for remote reference magnetotellurics, Geophysics, 44, 959-968, 1979.

Goldstein, M. A., and D. W. Strangway, Audio-frequency magnetotellurics with a grounded electric dipole source, Geophysics, 40, 669-683, 1975.

Goff, F. E., and J. N. Gardner, Geologic map of the Sulphur Springs geothermal system, Valles caldera, New Mexico, Los Alamos Scientific Laboratory Map, LA-8634-MAP, 2 sheets, 1980.

Goff, F., J. Gardner, R. Vidale, and R. Charles, Geochemistry and isotopes of fluids from Sulphur Springs, Valles caldera, New Mexico, J. Volcan. Geotherm. Res., 23, 273-297, 1985.

Goff, F., L. Shevenell, J. N. Gardner, F.-D. Vuataz, and C. O. Grigsby, The hydrothermal outflow plume of Valles caldera, New Mexico, and a comparison with other outflow plumes, J. Geophys. Res., 93, 6041-6058, 1988.

Goff, F., J. N. Gardner, J. B. Hulen, D. L. Nielson, R. Charles, G. WoldeGabriel, F.-D. Vuataz, J. A. Musgrave, L. Shevenell, and B. M. Kennedy, The Valles caldera hydrothermal system, past and present, New Mexico, USA, Scientific Drilling, 3, 181-204, 1992.

Heiken, G., F. Goff, J. N. Gardner, W. S. Baldridge, J. B. Hulen, D. L. Nielson, and D. Vaniman, The Valles/Toledo caldera complex, Jemez volcanic field, New Mexico, Annu. Rev. Earth Planet. Sci., 18, 27-53, 1990.

Hughes, L. J., and N. R. Carlson, Structure mapping at Trap Springs Oilfield, Nevada, using controlled-source magnetotellurics, First Break, 5, 403-418, 1987.

Hulen, J. B., and D. L. Nielson, 1986a, Stratigraphy and hydrothermal alteration in well Baca-8, Sulphur Springs area, Valles caldera, New Mexico, Geothermal Resources Council Trans., 10, 187-192, 1986a.

Hulen, J. B., and D. L. Nielson, 1986b, Hydrothermal alteration in the Baca geothermal system, Redondo Dome, Valles caldera, New Mexico, J. Geophys. Res., 91, 1967-1986, 1986b.

Hulen, J. B., and J. N. Gardner, Field geologic log for CSDP corehole VC-2B, Valles caldera, New Mexico, Rep. ESL-89025-TR, 92 pp., Univ. of Utah Res. Inst., Salt Lake City, 1989.

Hulen, J. B., D. L. Nielson, F. Goff, J. N. Gardner, and R. W. Charles, Molybdenum mineralization in an active geothermal system, Valles caldera, New Mexico, Geology, 15, 748-752, 1987.

Hulen, J. B., J. N. Gardner, D. L. Nielson, and F. Goff, Stratigraphy, structure, hydrothermal mineralization, and ore mineralization encountered in CSDP corehole VC-2A, Sulphur Springs area, Valles caldera, New Mexico - a detailed overview, Rep. ESL-88001-TR, 55 pp., Univ. of Utah Res. Inst., Salt Lake City, 1988.

Hulen, J. B., D. L. Nielson, and T. M. Little, Evolution of the western Valles caldera complex, New Mexico: evidence from intracaldera sandstones, breccias, and surge deposits, J. Geophys. Res., 96, 8127-8142, 1991.

Jiracek, G. R., C. Smith, and G. A. Dorn, Deep geothermal exploration in New Mexico using electrical resistivity, in Proc. Second United Nations Symp. on the Devel. and Use of Geothermal Resources, v. 2, 1095-1103, 1975.

Jiracek, G. R., W. S. Baldridge, and L. J. Hix, SAGE - A unique geophysical experience, The Leading Edge, Soc. Explor. Geophys., 45-49, March, 1991.

Keller, G. V., Rock and mineral properties, in Electromagnetic Methods in Applied Geophysics, edited by M. N. Nabighian, Soc. Explor. Geophys., Tulsa, Okla., 13-52, 1988.

Nielson, D. L., and J. B. Hulen, Internal geology and evolution of Redondo Dome, Valles caldera, New Mexico, J. Geophys. Res., 89, 8695-8711, 1984.

Olhoeft, G., Electrical properties of rocks, in Physical properties of rocks and minerals, ed. by Y. S. Touloukian and C. Y. Ho, McGraw-Hill/CINDAS Data Series on Material Properties, II-2, New York, 257-297, 1981.

Oristaglio, M. L., and M. H. Worthington, Inversion of surface and borehole electromagnetic data for two-dimensional electrical conductivity models, Geophys. Prospect., 28, 633-657.

Ostrander, A. G., Structural mapping at the Tomera Ranch oil field using CSAMT: a case history, Nevada Petroleum Society Fieldtrip Guidebook, 57-68, 1990.

Petrick, W. R., Pelton, W. H., and Ward, S. H., Ridge regression inversion applied to crustal sounding data from South Africa, Geophysics, 42, 995-1005, 1977.

Quist, A. S., and W. L. Marshall, The electrical conductances of aqueous sodium chloride solutions from 0 to 800 C and at pressures to 4000 bars, J. Phys. Chem., 71, 684-703, 1968.

Sandberg, S. K., and G. W. Hohmann, Controlled-source audiomagnetotellurics in geothermal exploration, Geophysics, 47, 100-116, 1982.

Smith, J. T., and J. R. Booker, Rapid inversion of two- and three-dimensional magnetotelluric data, J. Geophys. Res., 96, 3905-3922, 1991.

Smith, R. L., and R. A. Bailey, Resurgent cauldrons, in Studies in volcanology, ed. by R. R. Coats, R. L. Hay, and C. A. Anderson, Mem. Geol. Soc. Am., 116, 613-662, 1968.

Smith, R. L., R. A. Bailey, and C. S. Ross, Geologic map of the Jemez Mountains, New Mexico, U. S. Geol. Surv., Misc. Geol. Invest., Map I-571, 1970.

Stodt, J. A., Noise analysis for conventional and remote reference magnetotellurics, Ph.D. thesis, University of Utah, Salt Lake City, 220 pp., 1983.

Torres-Verdin, C., and F. X. Bostick, Jr., Principles of spatial surface electric field filtering in magnetotellurics: electro-magnetic array profiling (EMAP), Geophysics, 57, 603-622, 1992.

Vozoff, K., The magnetotelluric method, in Electromagnetic methods in applied geophysics, vol. 2B, Application, ed. by M. N. Nabighian, Soc. Explor. Geophys., Tulsa, 641-711, 1991.

Wannamaker, P. E., Resistivity structure of the Northern Basin and Range, in The role of heat in the development of energy and mineral resources in the Northern Basin and Range, Geothermal Resources Council Spec. Rep. 13, 345-363, 1983.

Wannamaker, P. E., Advances in three-dimensional magnetotelluric modeling using integral equations, Geophysics, 56, 1716-1728, 1991.

Wannamaker, P. E., G. W. Hohmann, and S. H. Ward, Magnetotelluric responses of three-dimensional bodies in layered earths, Geophysics, 49, 1517-1533, 1984.

Wannamaker, P. E., J. A. Stodt, and L. Rijo, Two-dimensional topographic responses in magnetotellurics modeled using finite elements, Geophysics, 51, 2131-2144, 1986.

Wannamaker, P. E., J. A. Stodt, and L. Rijo, A stable finite element solution for two-dimensional magnetotelluric modeling, Geophys. J. Roy. Astr. Soc., 88, 277-296, 1987.

Wannamaker, P. E., J. R. Booker, A. G. Jones, A. D. Chave, J. H. Filloux, H. S. Waff, and L. K. Law, Resistivity cross section through the Juan de Fuca subduction system and its tectonic implications, J. Geophys. Res., 94, 14,127-14,144, 1989.

Wannamaker, P. E., P. M. Wright, Z.-X. Zhou, X.-B. Li, and J.-X. Zhao, Magnetotelluric transect of Long Valley caldera: resistivity cross section, structural implications, and the limits of a two-dimensional analysis, Geophysics, 56, 926-940, 1991.

Wannamaker, P. E., and G. W. Hohmann, Electromagnetic induction studies, U. S. National Rep. to IUGG, Rev. Geophys., Supplement, 405-415, 1991.

Ward, S. H., W. T. Parry, W. P. Nash, W. R. Sill, K. L. Cook, R. B. Smith, D. S. Chapman, F. H. Brown, J. A. Whelan and J. R. Bowman, A summary of the geology, geochemistry and geophysics of the Roosevelt Hot Springs thermal area, Utah, Geophysics, 43, 1515-1542, 1978.

Ward, S. H., and W. R. Sill, Dipole-dipole resistivity surveys, Roosevelt Hot Springs KGRA, NSF Technical Rep., 76-2, Univ. of Utah, 29 pp., 1976.

Waxman, M. H., and L. T. M. Smits, Electrical conductivities in oil-bearing shaly sands, Trans Soc. Pet. Eng., 243, 107-123, 1968.

Wilds, S. R., and S. MacInnes, High resolution CSAMT applications in gold exploration - a case history, in Geology and ore deposits of the Great Basin, ed. by G. L. Raines, R. E. Lisle, R. W. Schafer, and W. H. Wilkinson, Geological Society of Nevada, vol. II, 1231-1236, 1991.

Wilt, M., and S. vonder Haar, A geological and geophysical appraisal of the Baca geothermal field, Valles caldera, New Mexico, J. Volcan. Geotherm. Res., 27, 349-370, 1986.

Zohdy, A. A. R., L. A. Anderson, and L. J. P. Muffler, Resistivity, self-potential, and induced polarization surveys of a vapor-dominated geothermal system, Geophysics, 38, 1130-1144, 1973.

Zonge, K. L., and L. J. Hughes, Controlled source audiomagnetotellurics, in Electromagnetic methods in applied geophysics, vol. 2B, Application, ed. by M. N. Nabighian, Soc. Explor. Geophys., Tulsa, 713-809, 1991.

Zonge, K. L., A. G. Ostrander, and D. F. Emer, Controlled source audio-frequency magnetotelluric measurements, in Magnetotelluric methods, ed. by K. Vozoff, Soc. Explor. Geophys., 749-763, 1986.

## FIGURES

1. Regional geological map of Valles caldera showing principal geological features and survey layout. Crossed-bipole transmitter antennae are about 13 km SSW of corehole VC-2B and Sulphur Springs (SS). CSAMT data was taken outside caldera on Schoolhouse Mesa (SM) and natural field MT data taken on Lake Mesa (LM). Fenton Hill hot dry rock prospect is FH and resurgent dome of Redondo Peak is RP. Geology primarily after Smith et al., (1970) and Hulen et al., (1991).

2. Detailed geology and CSAMT survey layout of Sulphur Springs area. Data was taken in four profiles designed to cross major structural features. Dots denote electrode positions (i.e., bipole spans along the profiles). Bipoles normal to profiles not drawn but were all 250 m in length. Stippling and geological labels are the same as for regional map. Geology after Goff and Gardner (1980) and Hulen et al., (1991).

3. East-west geologic cross section based upon surface mapping and drill core logs. Distributed normal faulting between wells VC-2A and WC-24 is not well constrained. Section may be compared to geological inferences based on resistivity data. Replotted from Goff et al. (1992).

4. Schematic of tensor CSAMT measurement setup. For the scalar approach, the broadside configuration is typical where source and electric field sensor bipoles are parallel and the electric field is measured along the profile. For the tensor approach, the coincident source configuration is shown as it is the most feasible and was undertaken at Sulphur Springs.

5. Example far-field through near-field CSAMT responses over a uniform half-space (top) and a four-layered earth (bottom). The layered earth section may be roughly representative of that at Sulphur Springs, but the former would be scaled down in dimensions by a factor of ten (i.e., frequency response shifted upward by 100).

6. Tensor CSAMT data taken about 125 m SE of VC-2B compared to natural field MT data taken by G. R. Jiracek. Error intervals are nominally one standard deviation. Square symbols denote MT data. Near-field effects in CSAMT results appear to occur at 1 and 2 Hz especially in the phase. The x-axis is N45°E and y-axis is S45°E for all periods. Goodness-of-fit of TM mode response of the 2-D resistivity model of Figure 11 is plotted as the solid curves.

7. Pseudosections of nominal TE (xy-mode) apparent resistivity and impedance phase for central line N1 crossing VC-2B corehole. Contour intervals are 0.2 log units in $\rho_a$ and 5° in phase. Contours are plotted from endpoint to endpoint of the profile and are based hand-smoothed sounding values.

8. Pseudosections of nominal TM (yx-mode) apparent resistivity and impedance phase for central line N1 crossing VC-2B corehole. Contour intervals are 0.2 log units in $\rho_a$ and 5° in phase. Contours are plotted from endpoint to endpoint of the profile and are based hand-smoothed sounding values.

9. Pseudosections of complex tipper elements $M_{zy}$ (TE mode, top) and $M_{zx}$ (bottom) for central line N1 crossing VC-2B corehole. Contour intervals are 5% for all quantities. Dashed contours denote negative values. Contours are plotted from endpoint to endpoint of the profile and are based hand-smoothed sounding values.

10. Tensor CSAMT data taken on Schoolhouse Mesa merged with natural field MT data taken by G. R. Jiracek (error bars plus square symbols). Error intervals are nominally one standard deviation. Tensor CSAMT calculations for best-fit, five layer model are shown with solid and long dashed lines, while MT calculations for this model are shown with short dashed curves. CSAMT calculation for xy-mode with conductive layer at 235 m depth constrained to be 625 m thick is shown as curves of medium dashes. The x-axis is true north and the y-axis is true east for all periods.

11. Best-fit two-dimensional resistivity model of line N1 across the VC-2B well site derived primarily by trial-and-error forward modeling. Details of the finite element mesh geometry have been preserved but resistivities have been grouped into half-decade intervals for simplicity. There is no vertical exageration. Sounding VCN1E1 shown in Figure 6 is site 8 in this section, while sounding VCN1E3 shown in Figure 13 is site 10 here. Goodness-of-fit of the TM mode response of the 2-D model to the data is exemplified with these sounding plots.

12. Amplitudes of major axes of E- and H-field ellipses at Schoolhouse Mesa site as a function of frequency for both source bipoles. Observed fields are shown as two standard deviation error intervals while calculated amplitudes are shown as solid and dashed curves. Calculations consider the 1-D resistivity model derived through inversion of the data of Figure 10.

13. Tensor CSAMT data at site VCN1E3 with TM mode response of 2-D model of Figure 11 plotted as solid curves. Fit of 1-D tensor CSAMT inversion to the data is shown as curves of long dashes (yx-mode). Also shown is tensor CSAMT response using layered model from Schoolhouse Mesa interpretation (curve of short dashes, yx-mode).

14. Amplitudes of major axes of E- and H-field ellipses at site 10 along profile N1 as a function of frequency for source bipole 1. Observed fields are shown as two standard deviation error intervals. Curves of long dashes are the 1-D response of the resistivity section immediately below site 10 from the inversion of Figure 13. Curves of short dashes are the 1-D response of the resistivity section derived from inversion of the Schoolhouse Mesa data (Figure 10). Solid curves are 1-D response of layered model identical to Schoolhouse Mesa profile but with the Paleozoic sedimentary section similar to that inferred below site 10. Parameters of this latter model are listed on the figure.

15. Observed electric (E) and magnetic (H) field major and minor ellipse axes at 128 Hz over the Sulphur Springs survey area. Ellipses are plotted for both source bipoles as labeled in Figure 1. Error intervals in ellipse length and orientation are one standard deviation and are derived through repeat measurements.

16. Computed electric (E) and magnetic (H) field major and minor ellipse axes at 128 Hz over the Sulphur Springs survey area using the composite layered earth model interpreted from the data at site 10 on line N1 to control field amplitudes. Ellipses are plotted for both source bipoles as labeled in Figure 1.

17. Observed and computed H-field ellipse axes at 1 Hz over the Sulphur Springs survey area. Plot shows pronounced elliptical polarization in the data which is not observed in the model.

18. Example soundings comparing scalar and tensor apparent resistivities at two sites on line N1. Upper panels show xy quantities while lower panels show yx. Scalar results are shown with box symbols plus error bars while tensor results are shown as error intervals only. At site 24, tensor results are nearly coincident with lower scalar data (tensor errors seen protruding below solid scalar symbols). Transmitter bipole number giving rise to each scalar curve is denote 1 or 2 as labeled in Figure 1.

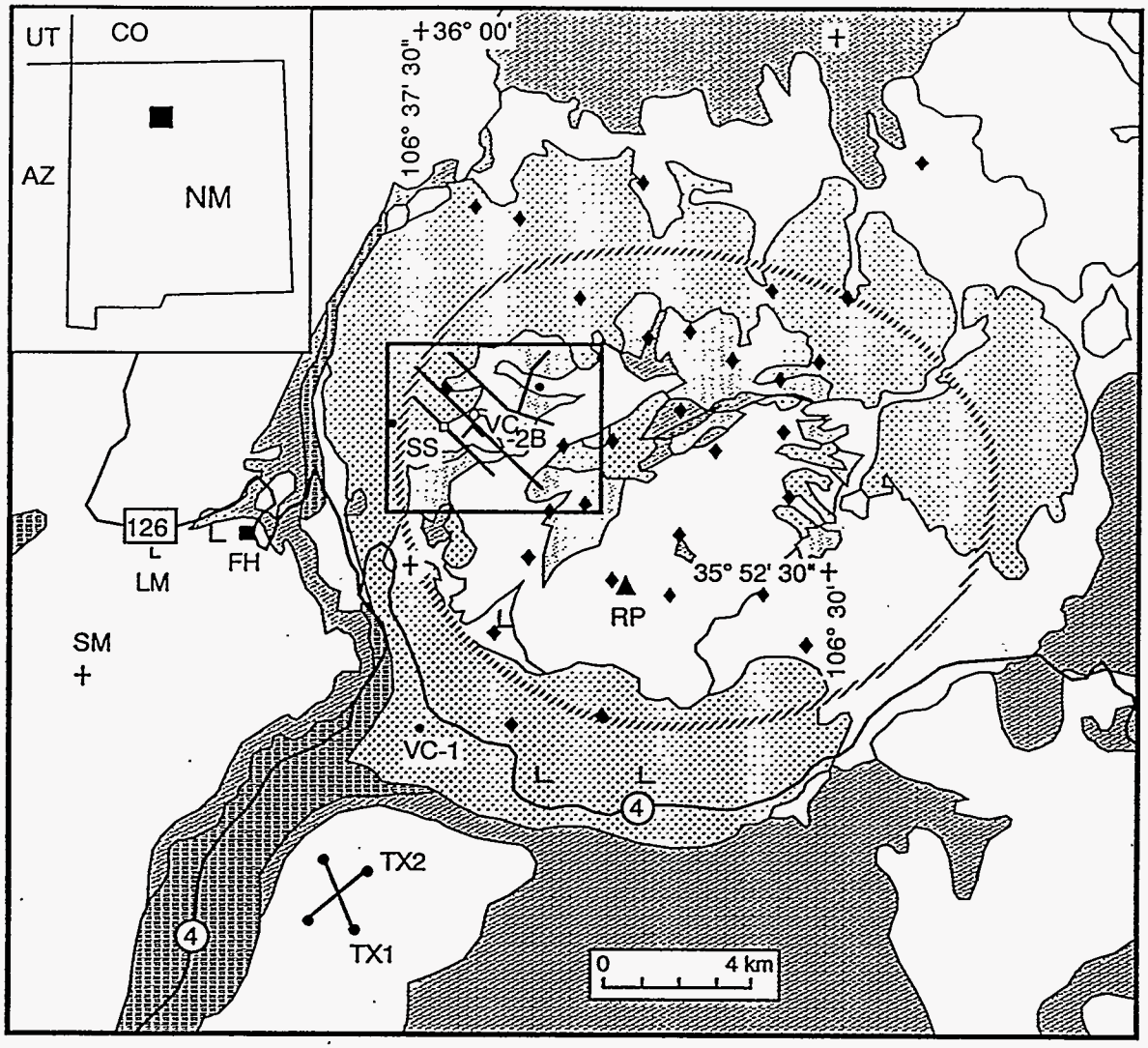


Surficial deposits, undivided; incl. lacustrine and landslides

Caldera-fill deposits, unsorted (Pleistocene)

Valles Rhyolite; domes, flows, and tuffs; incl. resurgent dome

Bandelier Tuff and associated ignimbrites

Pre-caldera volcanics (Miocene-Pliocene)

Penn.-Perm. siliciclastic and carbonate rocks

1.

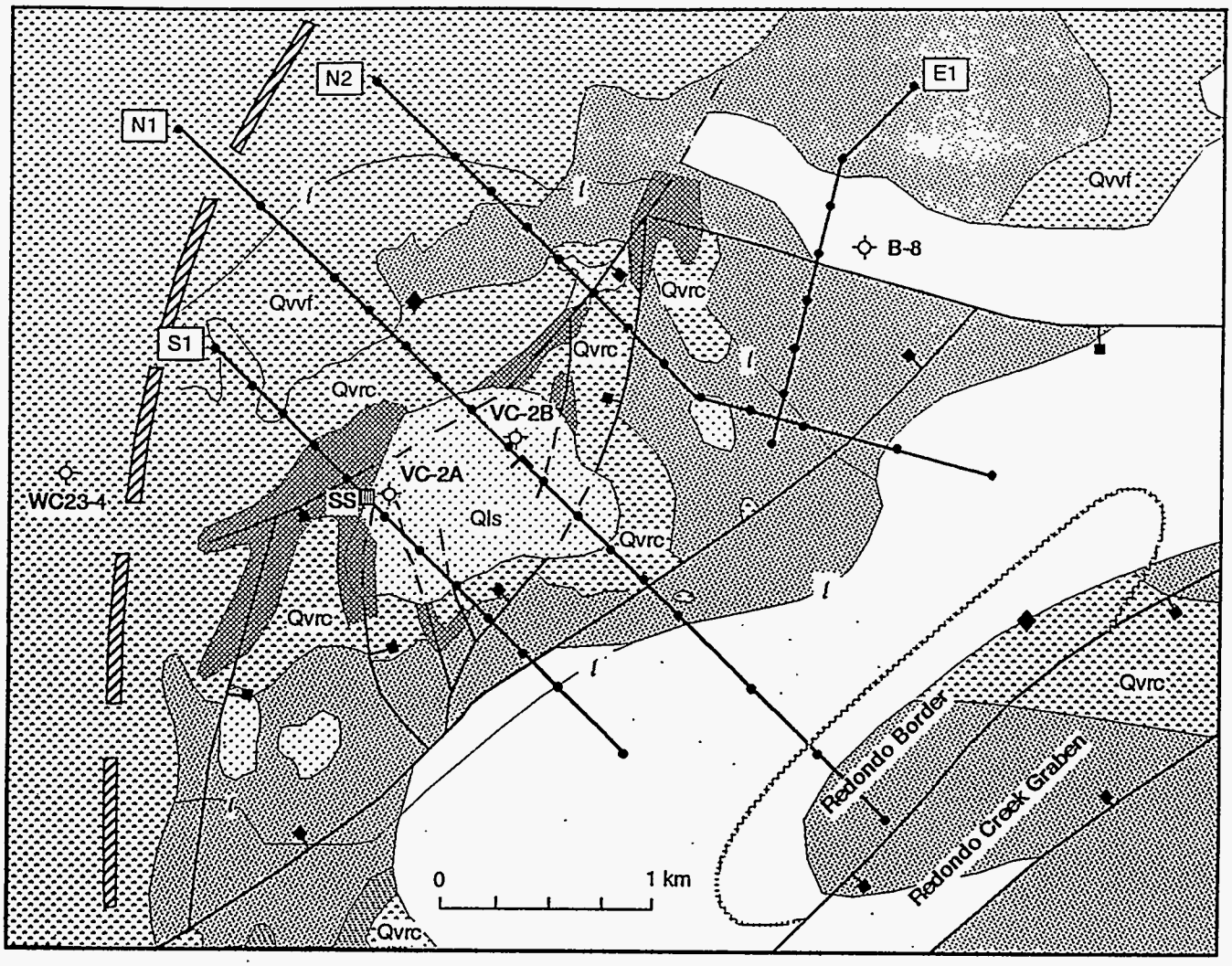


CSAMT profile
(dots mark electrode positions)

VC-2B
Drill collar
location

Surficial acid -
sulfate alteration

Fault, square on
down-thrown side

Limits of detailed
mapping of Goff and
Gardner (1980)

Caldera structural
margin (ring-fracture
system)

Stippling as for regional map

2.

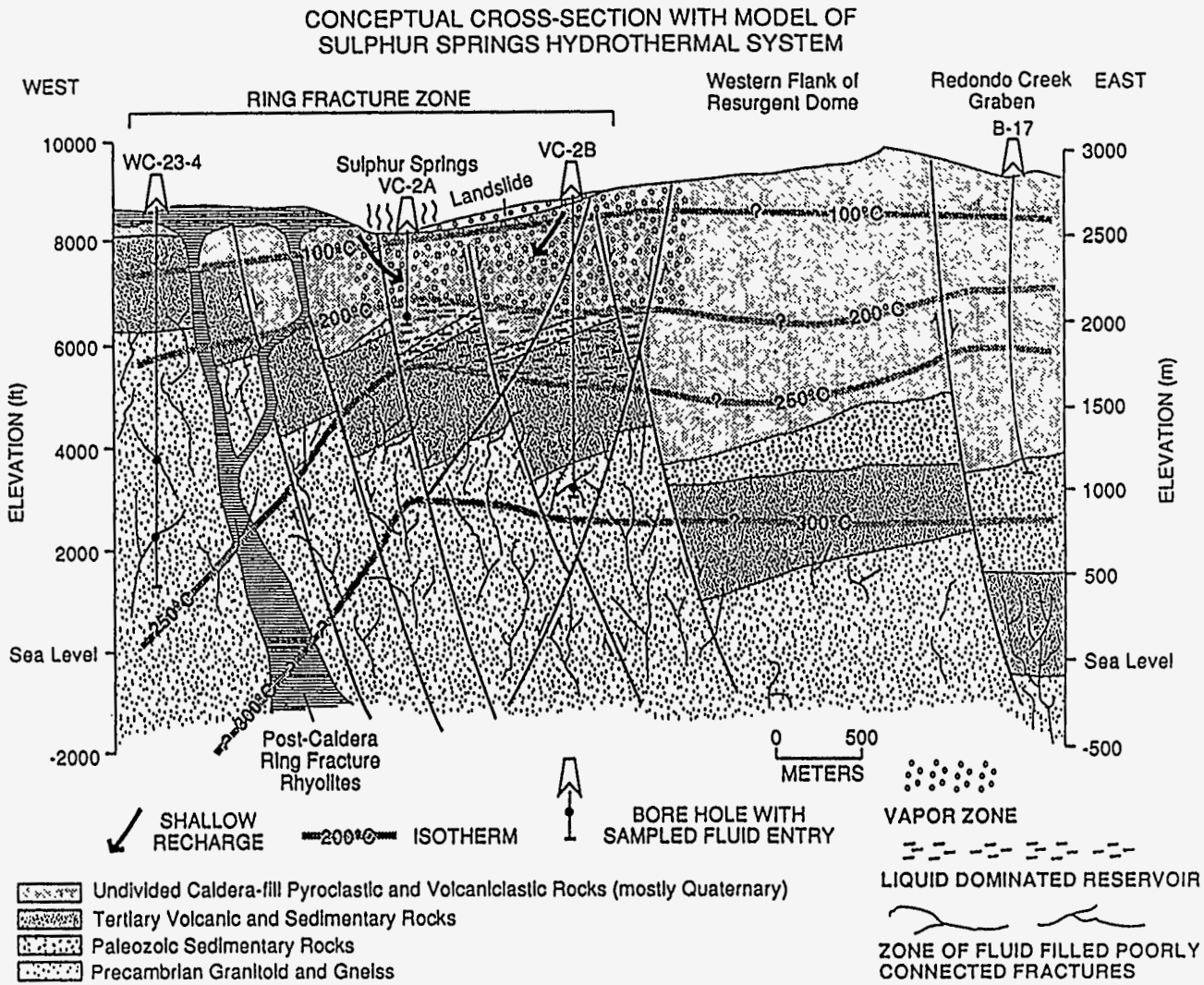


Fig. 3: Cross-section of Sulphur Springs sub-system, Valles hydrothermal system showing detailed configuration of a major upflow zone in the caldera (from Gardner et al., 1989).

# CSAMT Deployment

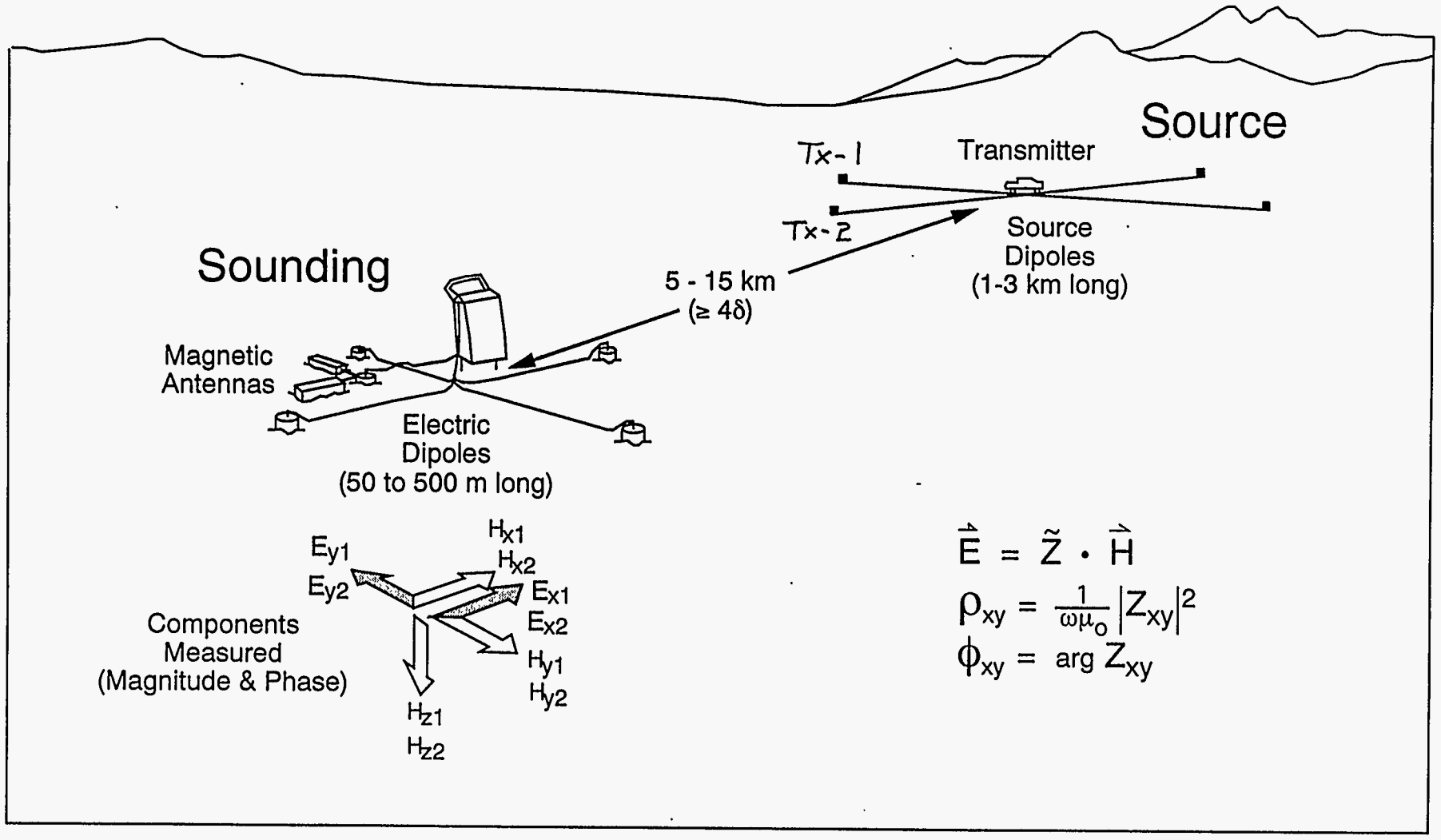


$$\vec{E} = \tilde{Z} \cdot \vec{H}$$

$$\rho_{xy} = \frac{1}{\omega \mu_o} |Z_{xy}|^2$$

$$\phi_{xy} = \arg Z_{xy}$$

## Homogeneous Earth

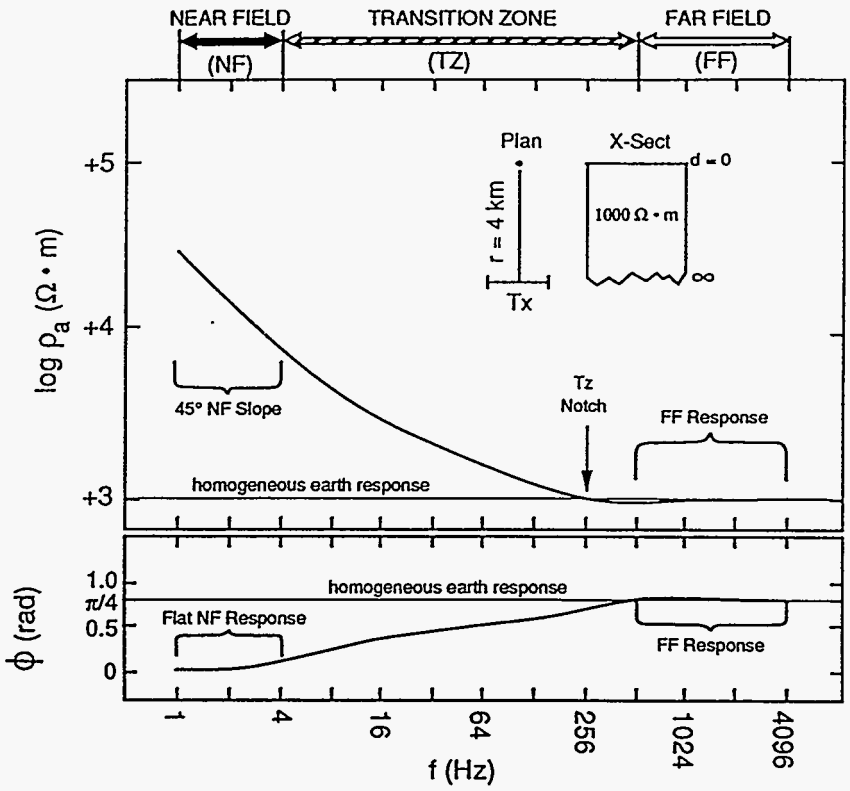


## Layered Earth

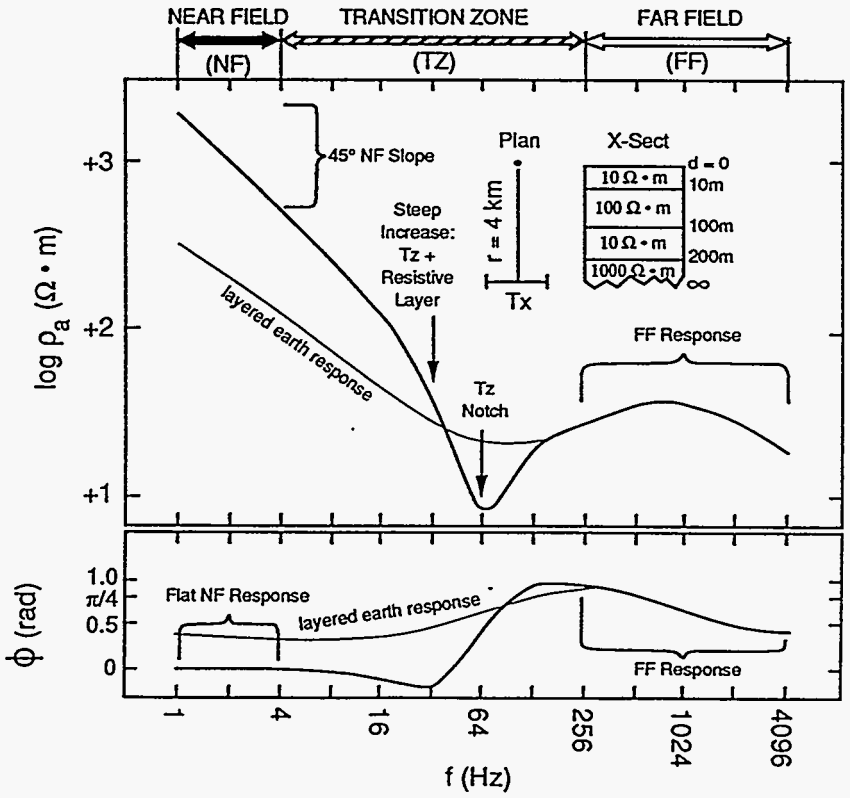


5.

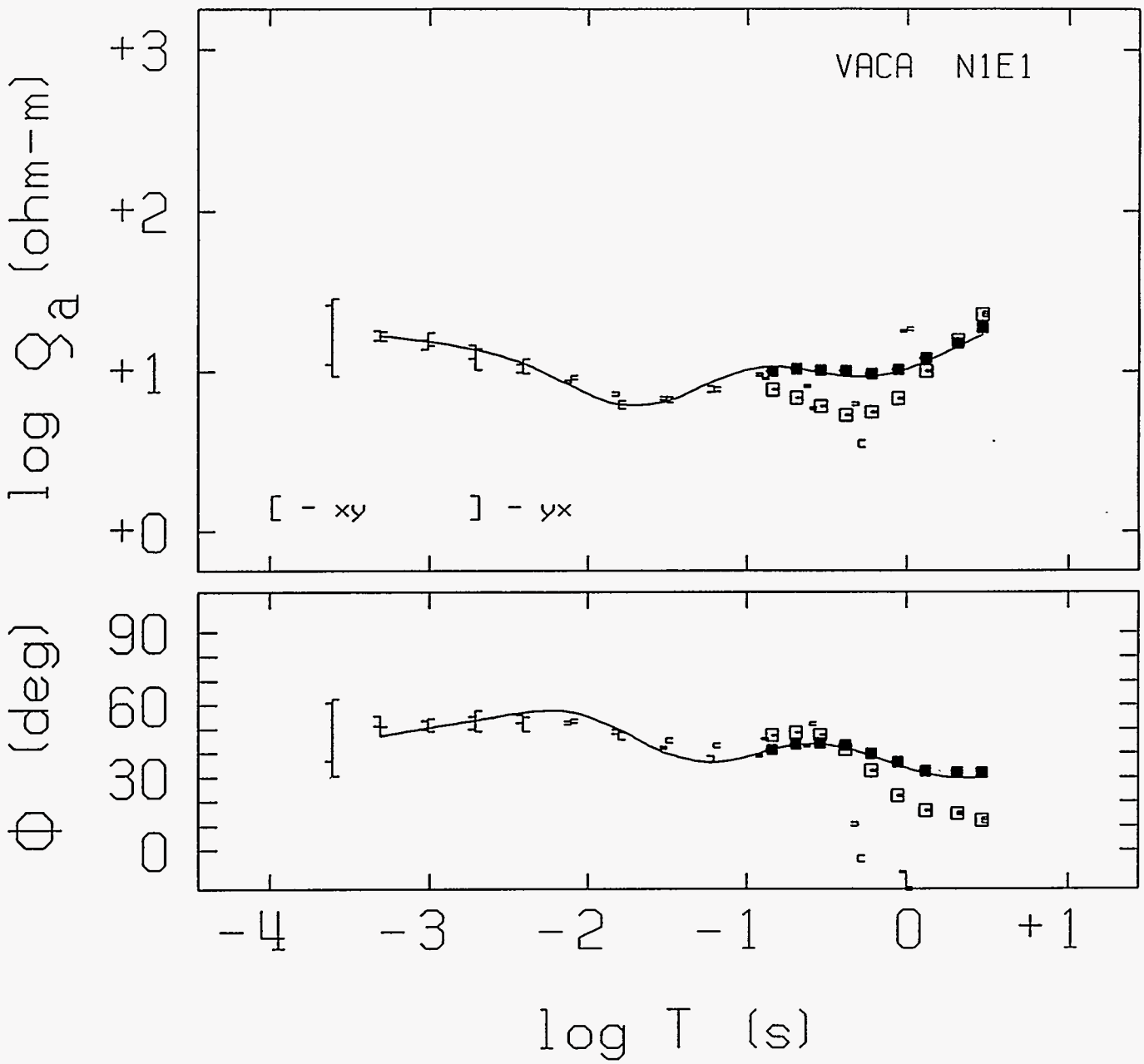
VACA N1E1
log ρa (ohm-m)
+3
+2
+1
+0
[ - xy
] - yx
Φ (deg)
90
60
30
0
-4
-3
-2
-1
0
+1
log T (s)

7.

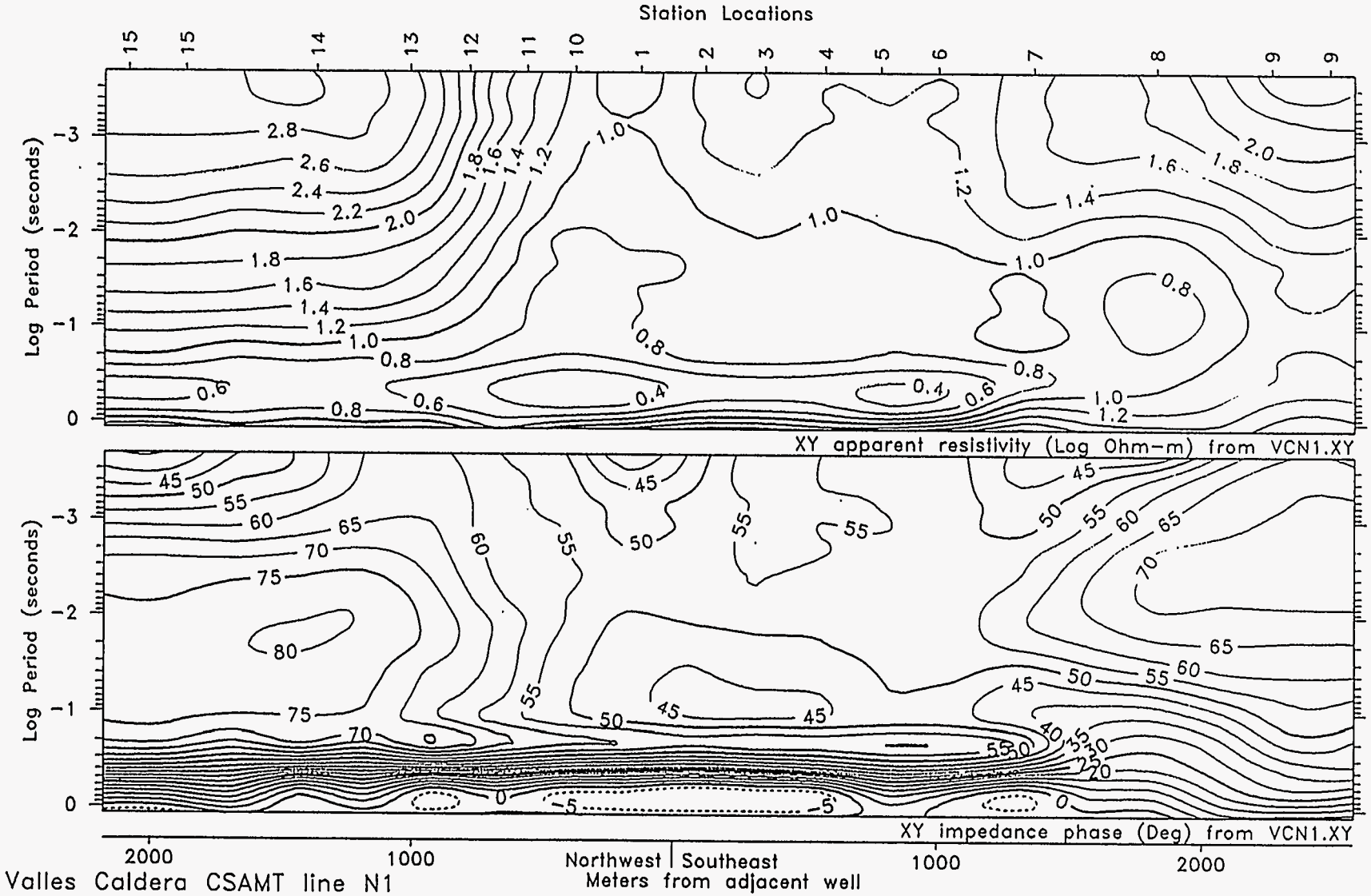


Valles Caldera CSAMT line N1

8.

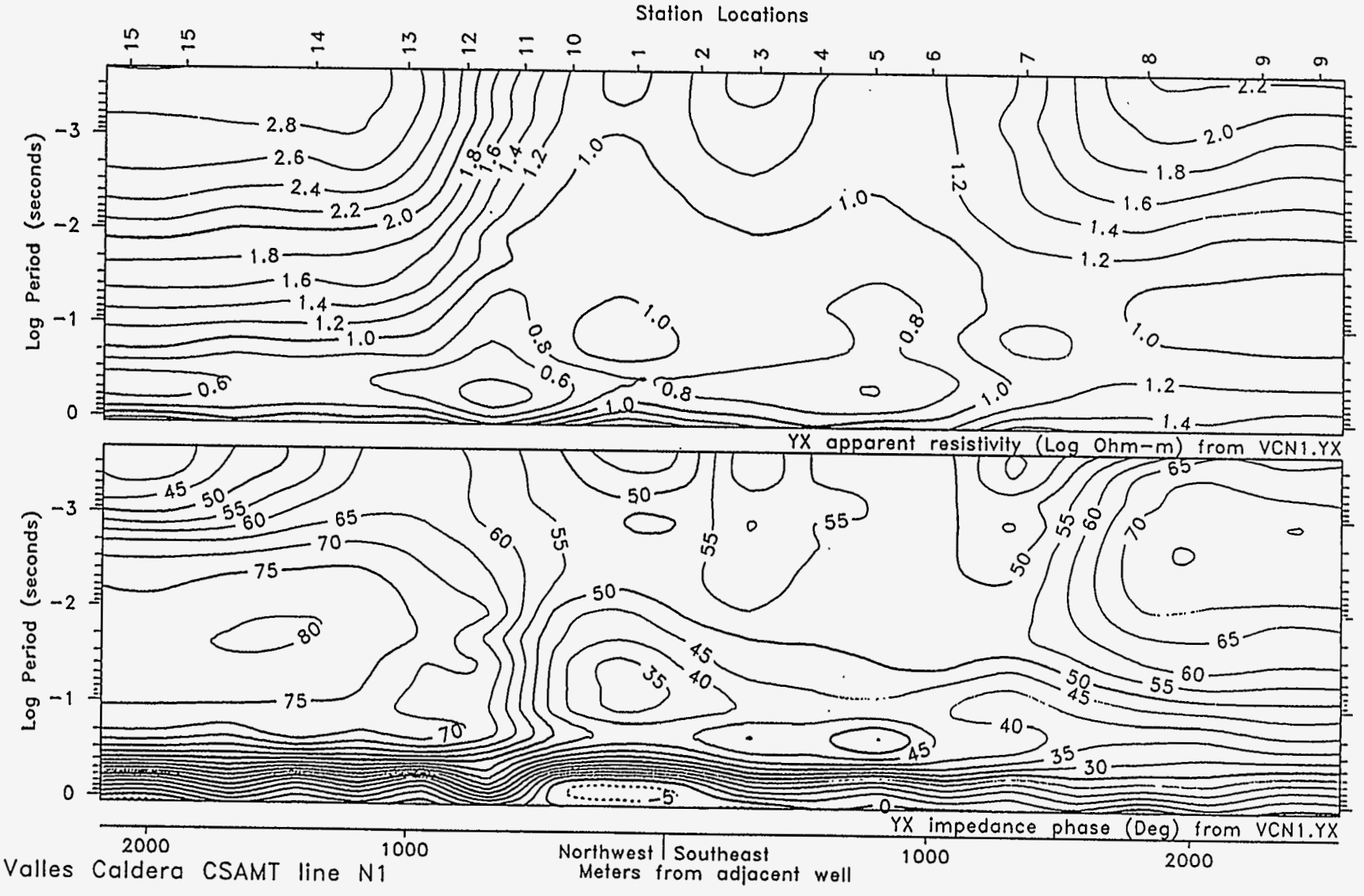


Valles Caldera CSAMT line N1

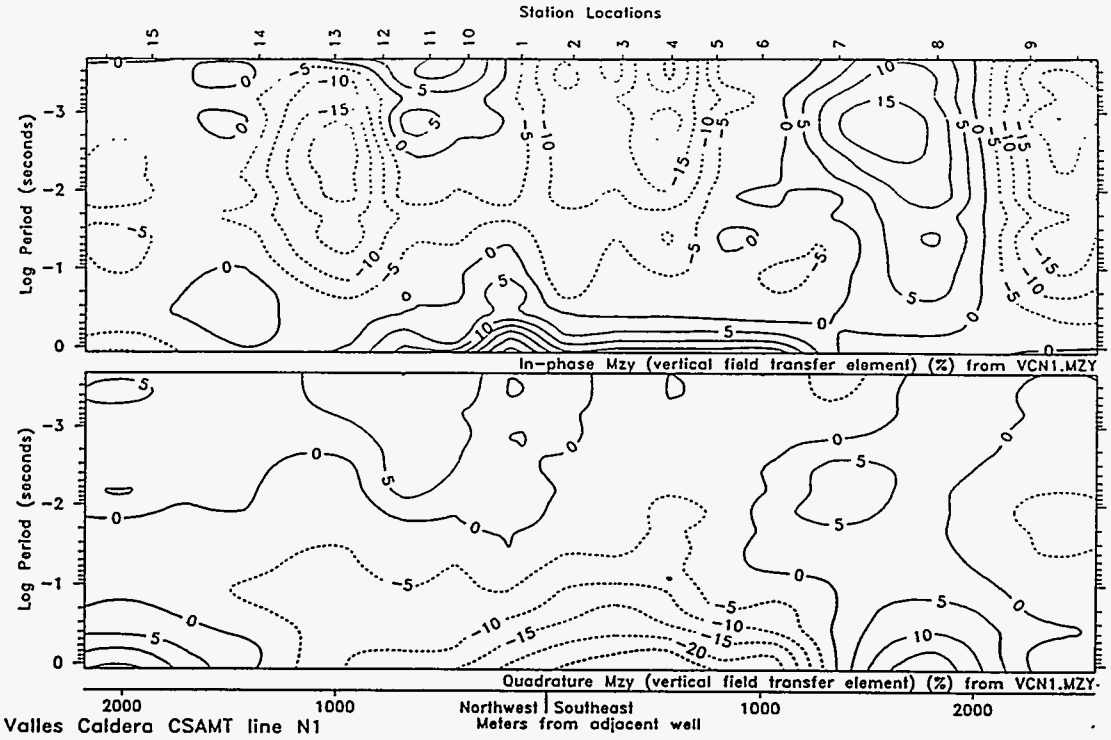
Station Locations
Log Period (seconds)
In-phase Mzy (vertical field transfer element) (%) from VCN1.MZY
Quadrature Mzy (vertical field transfer element) (%) from VCN1.MZY
2000
1000
Northwest | Southeast
1000
2000
Meters from adjacent well
Valles Caldera CSAMT line N1

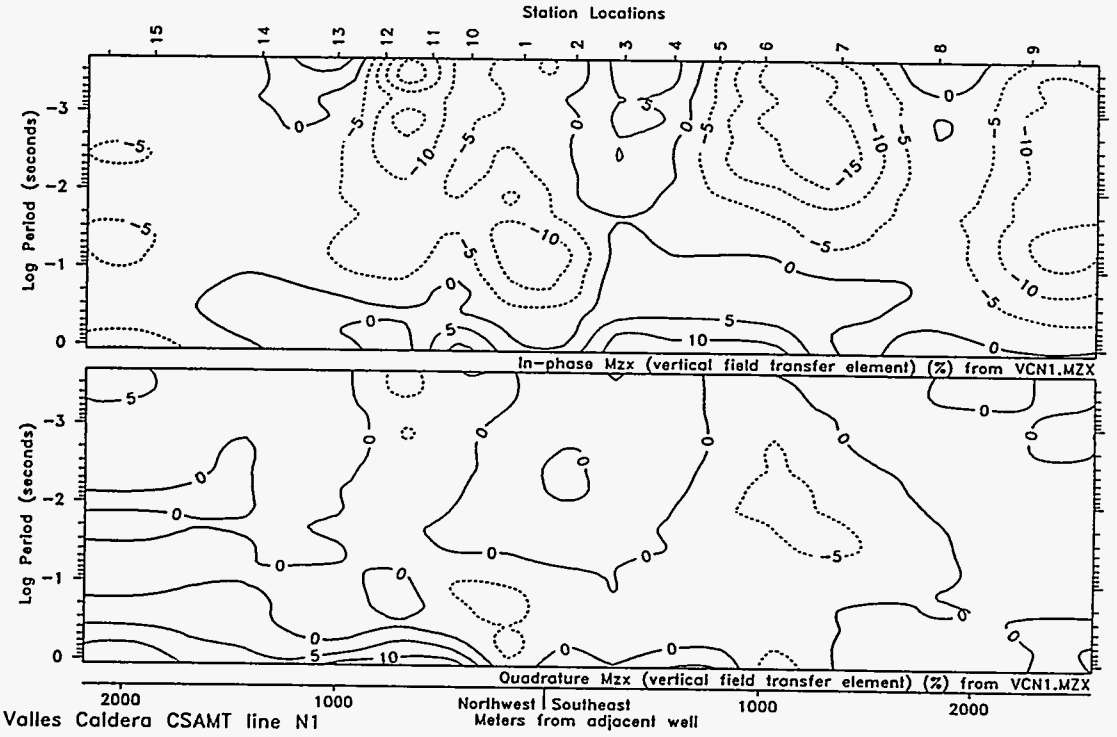
Station Locations
Log Period (seconds)
In-phase Mzx (vertical field transfer element) (%) from VCN1.MZX
Quadrature Mzx (vertical field transfer element) (%) from VCN1.MZX
2000
1000
Northwest | Southeast
1000
2000
Meters from adjacent well
Valles Caldera CSAMT line N1

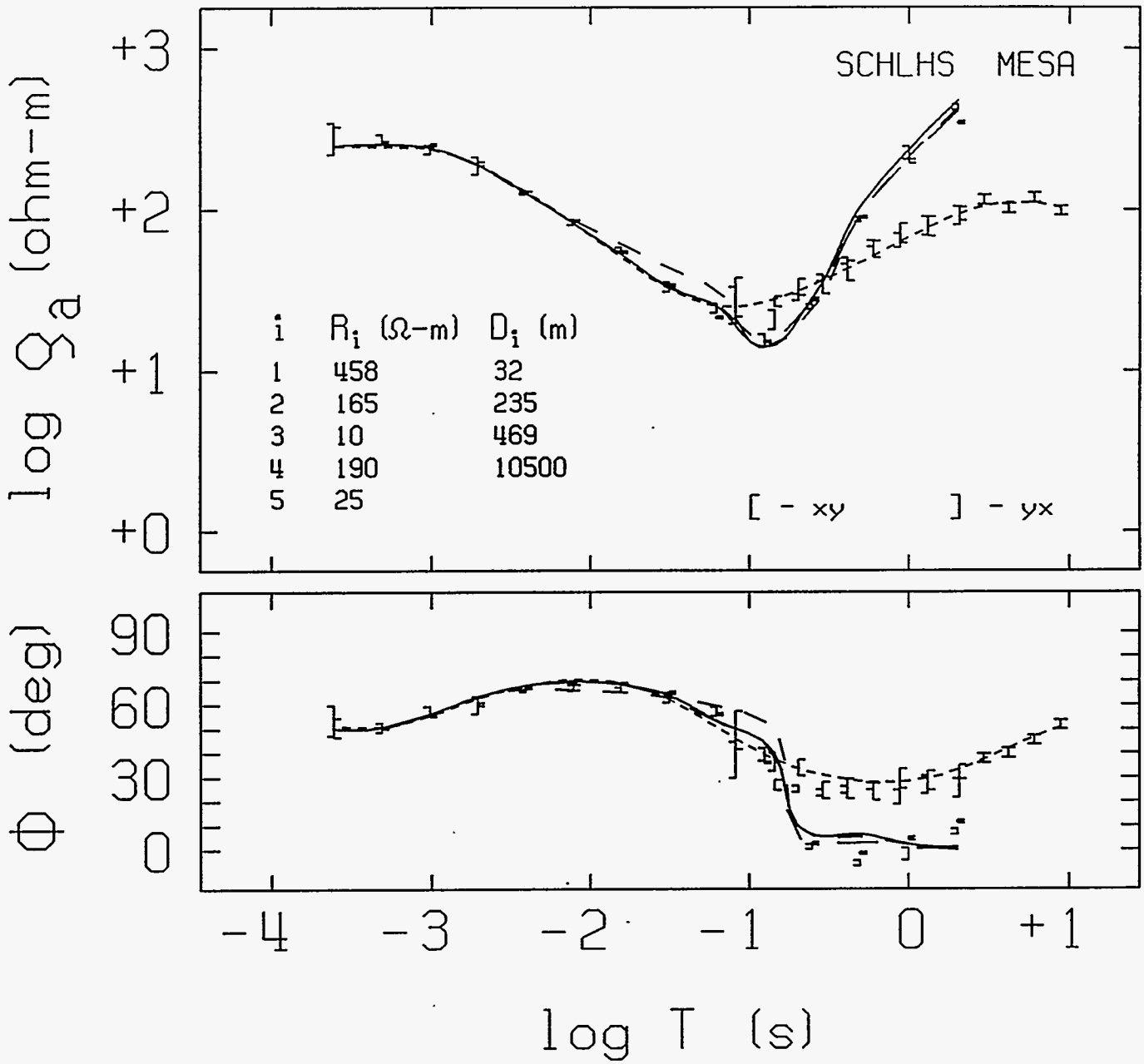
SCHLHS MESA
log ρa (ohm-m)
+3
+2
+1
+0
i Ri (Ω-m) Di (m)
1 458 32
2 165 235
3 10 469
4 190 10500
5 25
[ - xy
] - yx
Φ (deg)
90
60
30
0
-4
-3
-2
-1
0
+1
log T (s)

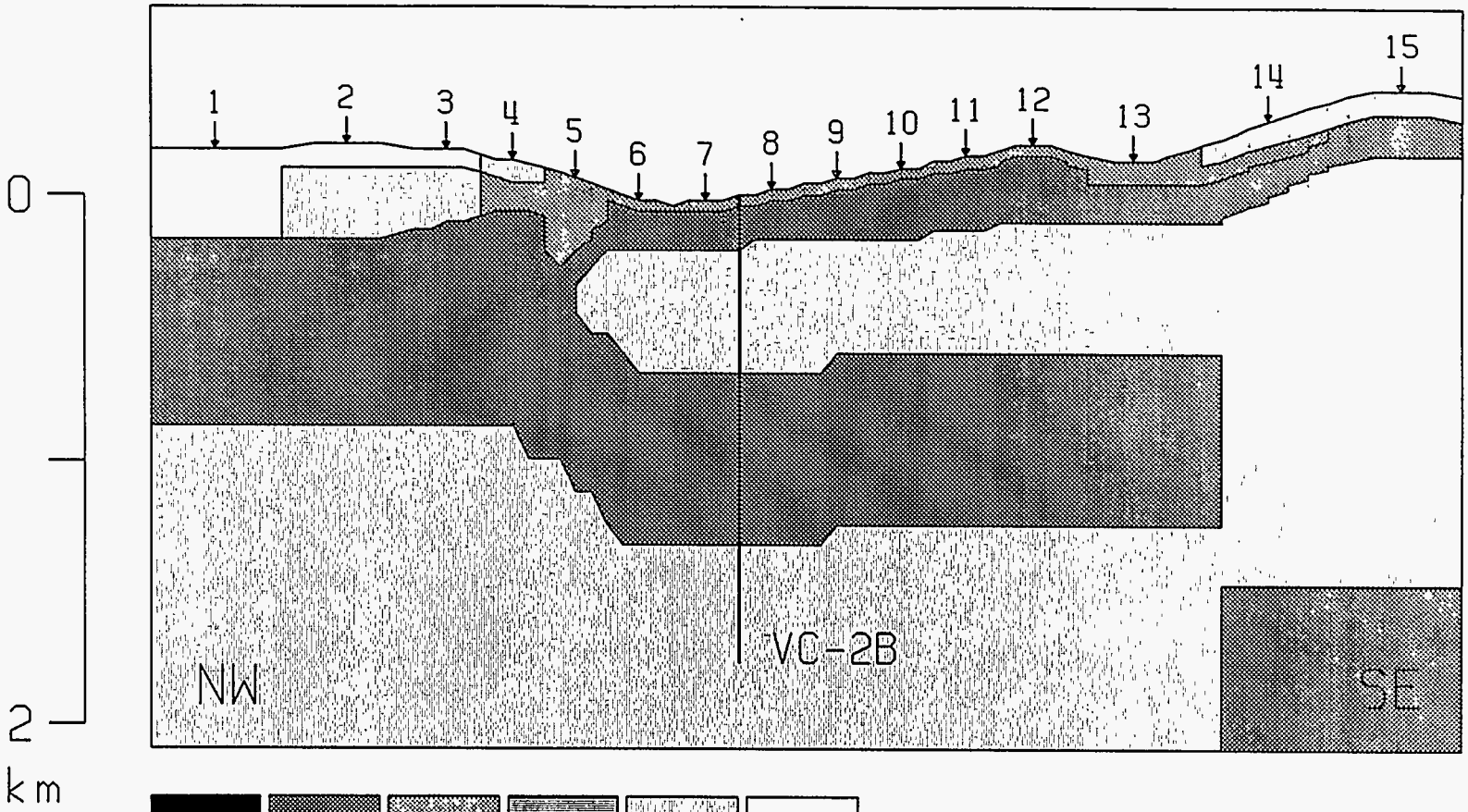
1
2
3
4
5
6
7
8
9
10
11
12
13
14
15
0
2
km
NW
VC-2B
SE
ρ (Ω-m)
≤3.2
≤10
≤32
≤100
≤320
≤10³
VACA-SLSP-N1
0
1.3 km

11.

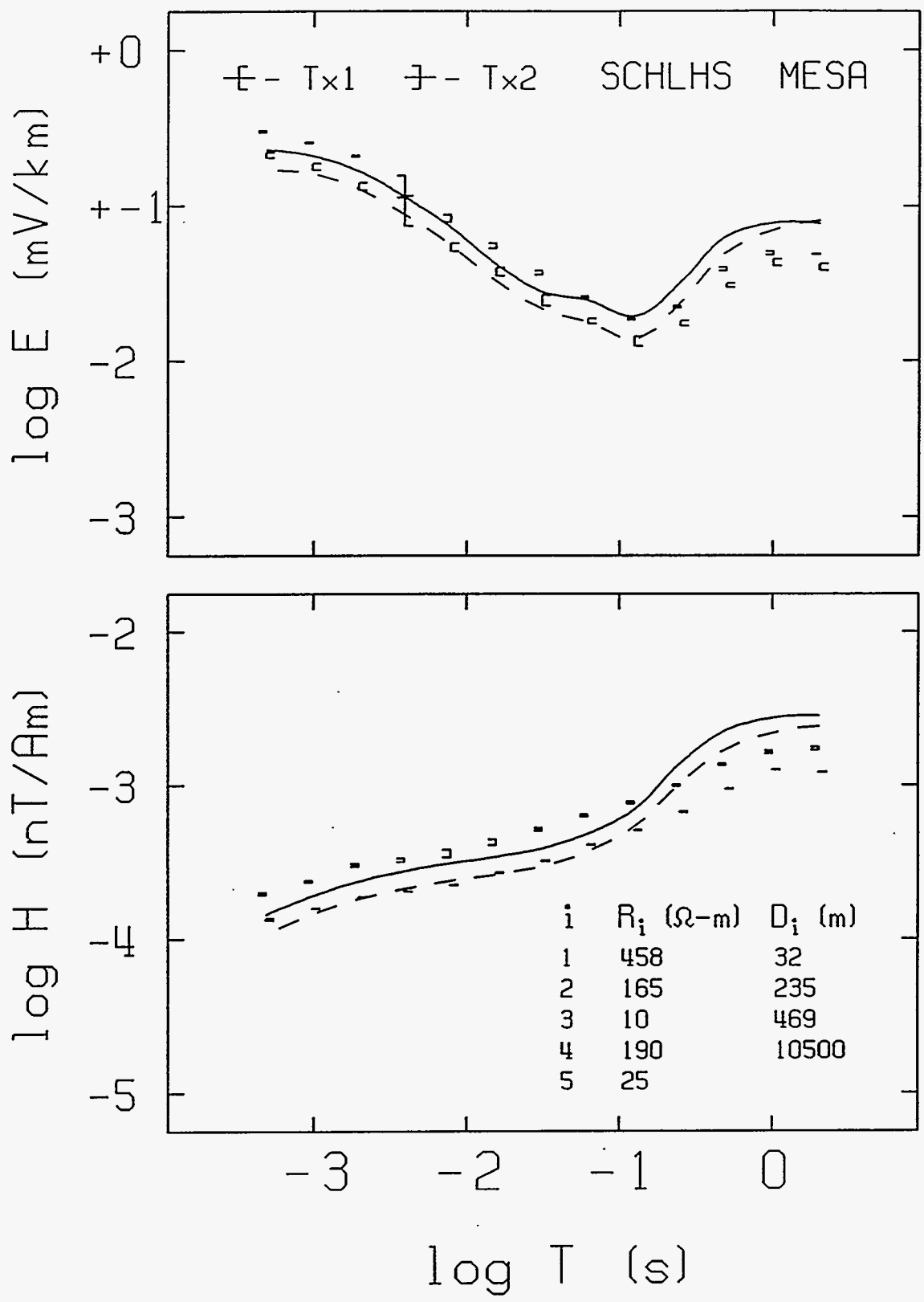
+0
+-1
-2
-3
log E (mV/km)
+- Tx1
+- Tx2
SCHLHS MESA
-2
-3
-4
-5
log H (nT/Am)
i R_i (Ω-m) D_i (m)
1 458 32
2 165 235
3 10 469
4 190 10500
5 25
-3 -2 -1 0
log T (s)

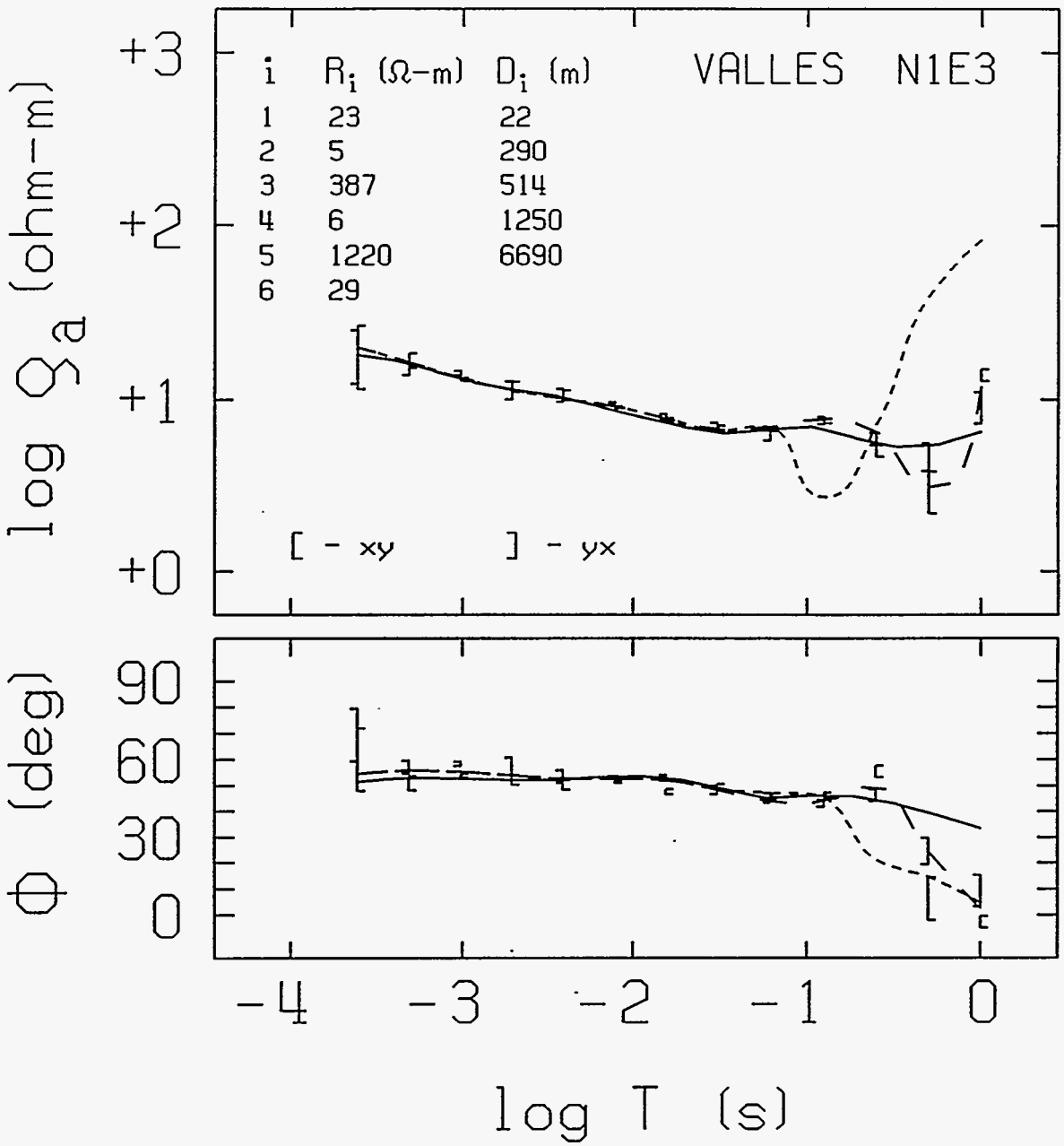
VALLES N1E3
i R_i (Ω-m) D_i (m)
1 23 22
2 5 290
3 387 514
4 6 1250
5 1220 6690
6 29
[ - xy ] - yx
log ρa (ohm-m)
+3
+2
+1
+0
Φ (deg)
90
60
30
0
-4
-3
-2
-1
0
log T (s)

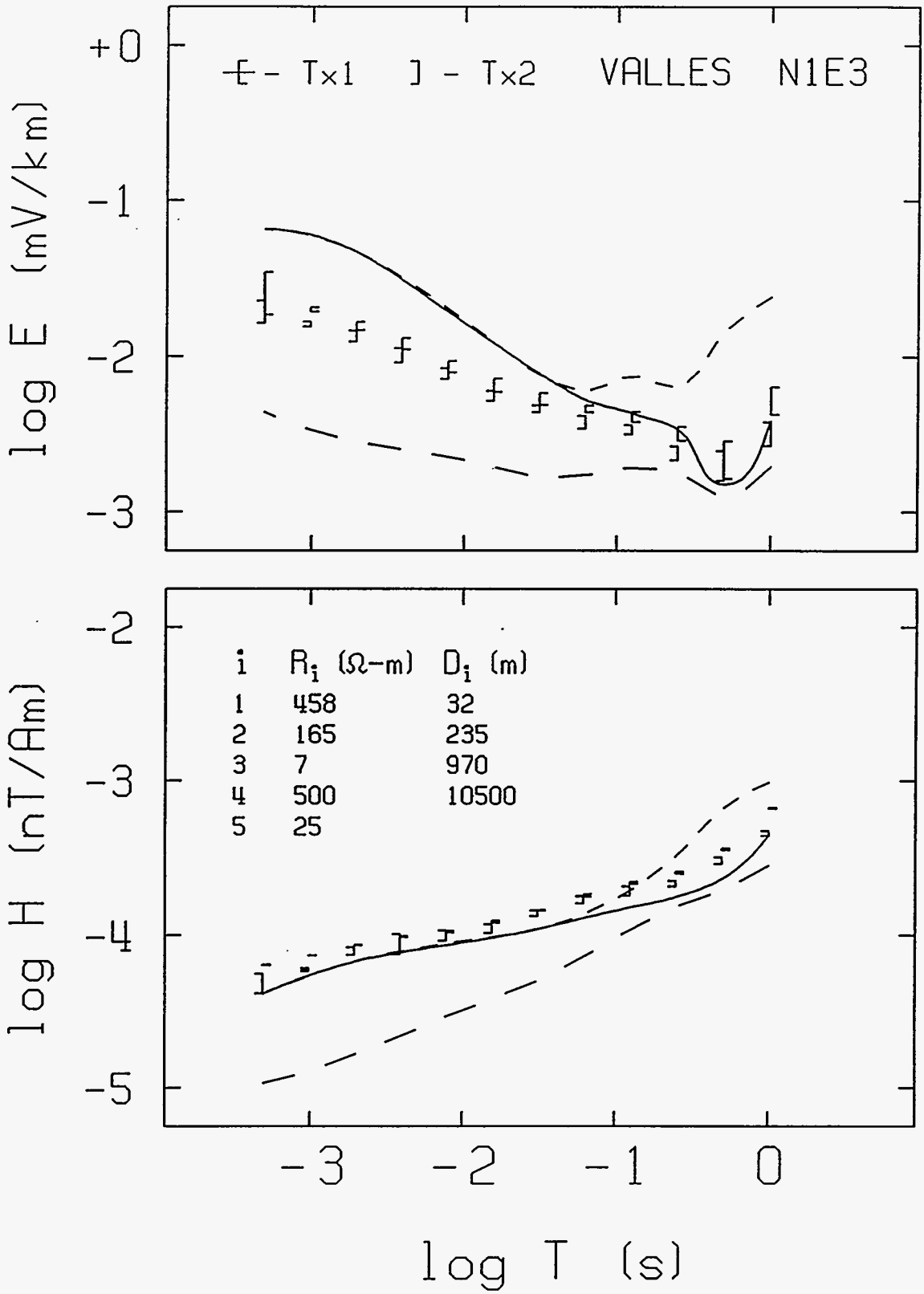
+0
-1
-2
-3
log E (mV/km)
T×1 - T×2 VALLES N1E3
-2
-3
-4
-5
log H (nT/Am)
i R_i (Ω-m) D_i (m)
1 458 32
2 165 235
3 7 970
4 500 10500
5 25
-3 -2 -1 0
log T (s)

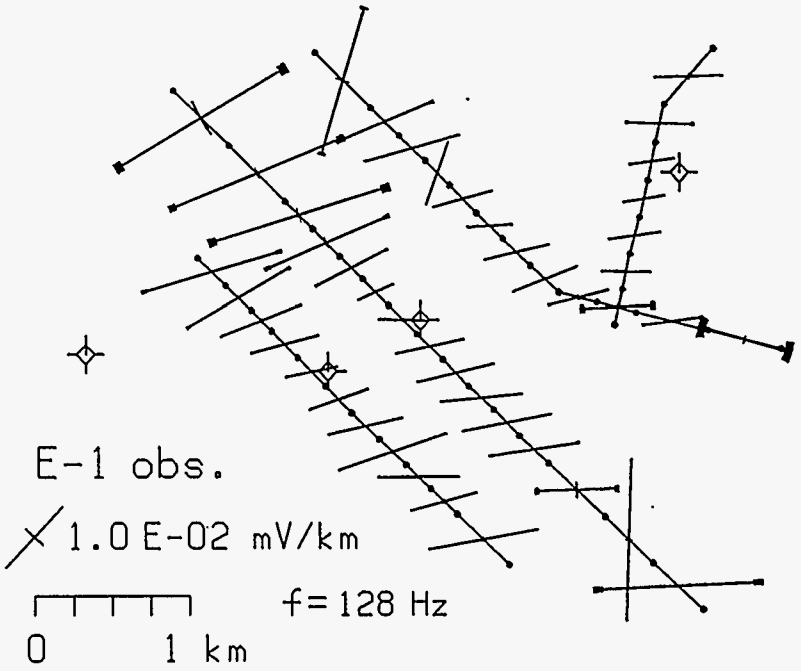
E-1 obs.
1.0 E-02 mV/km
f= 128 Hz
0
1 km

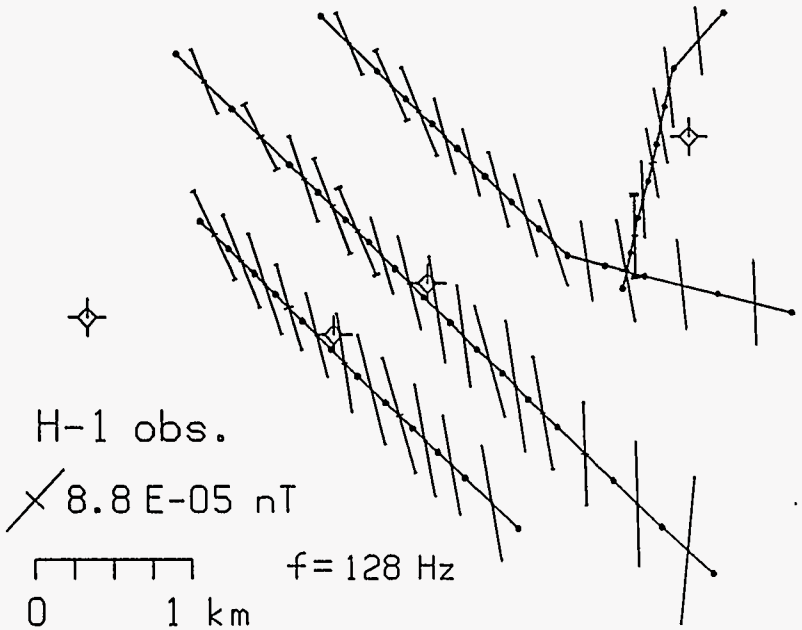
H-1 obs.
8.8 E-05 nT
f= 128 Hz
0
1 km

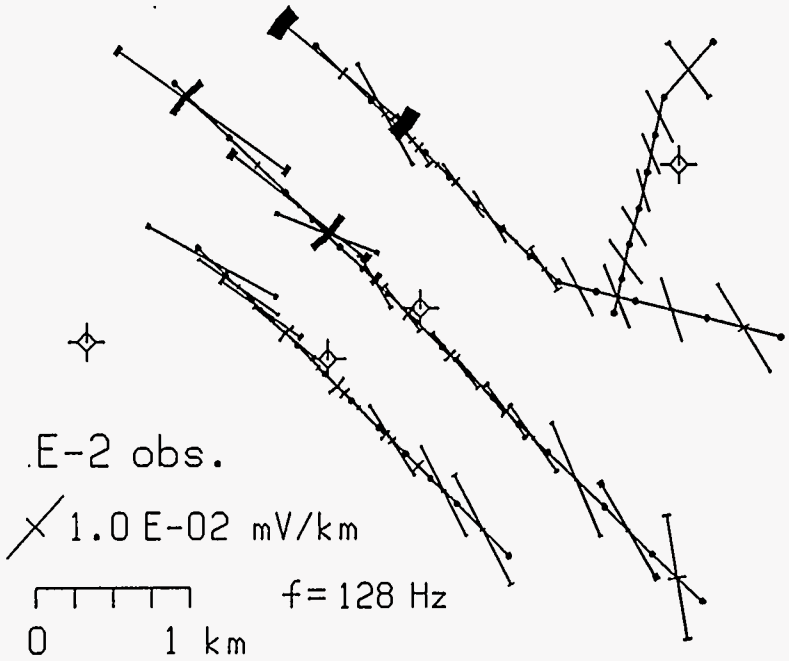
E-2 obs.
1.0 E-02 mV/km
f= 128 Hz
0
1 km

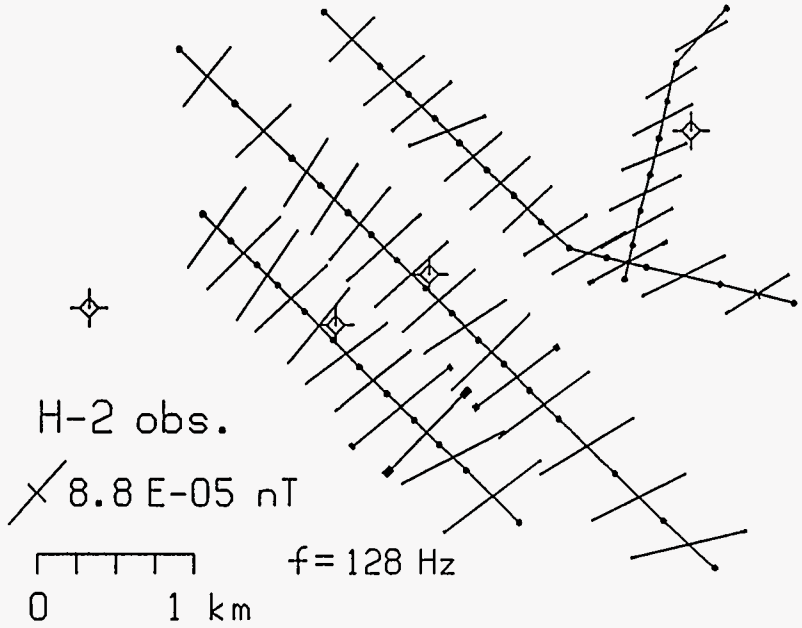
H-2 obs.
8.8 E-05 nT
f= 128 Hz
0
1 km

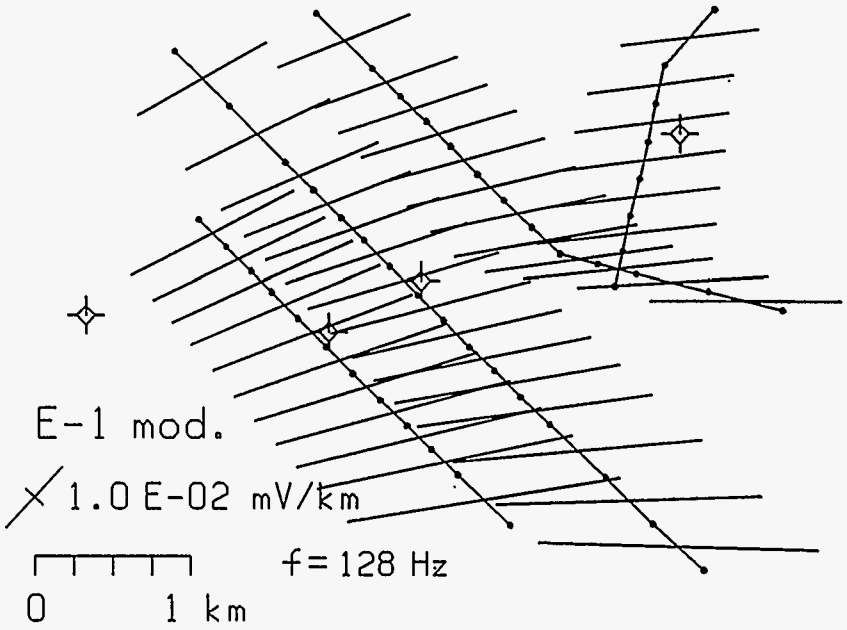
E-1 mod.
1.0 E-02 mV/km
f = 128 Hz
0
1 km

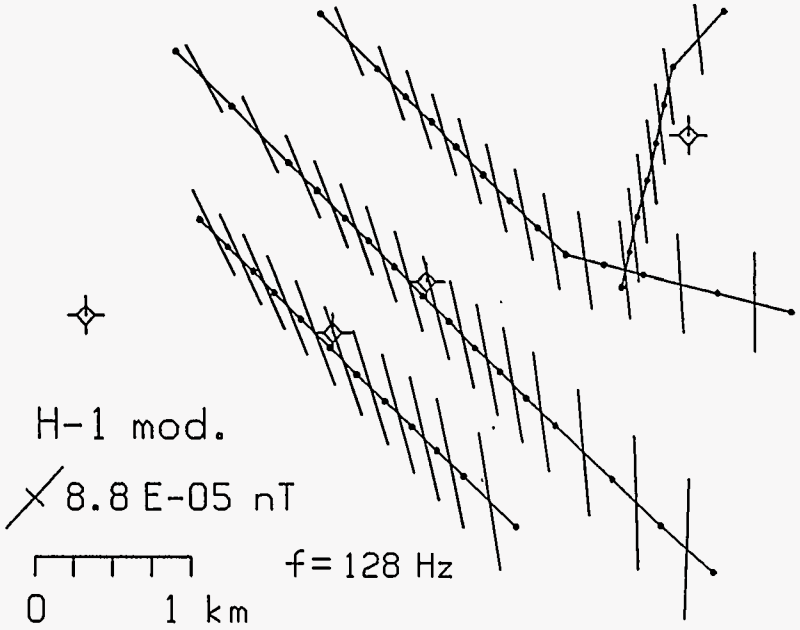
H-1 mod.
8.8 E-05 nT
f = 128 Hz
0
1 km

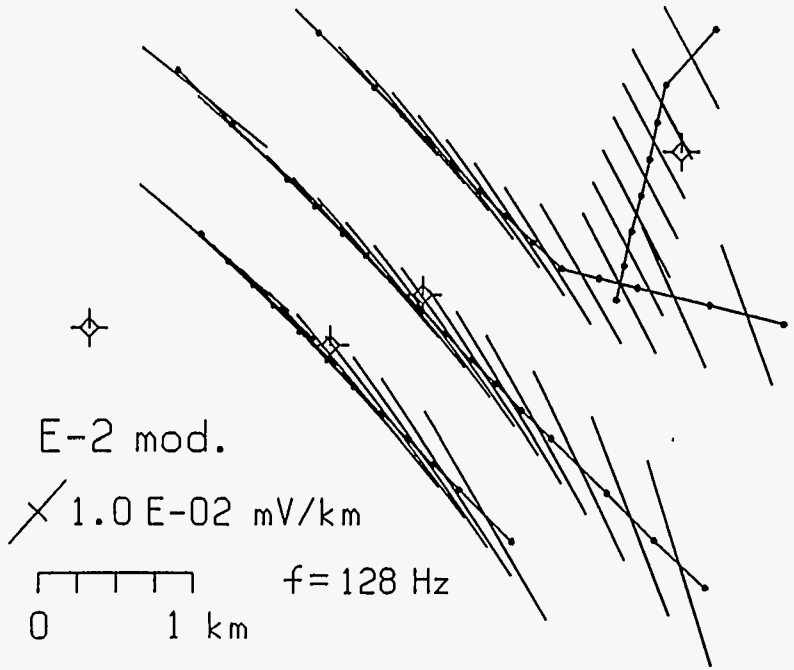
E-2 mod.
1.0 E-02 mV/km
f = 128 Hz
0
1 km

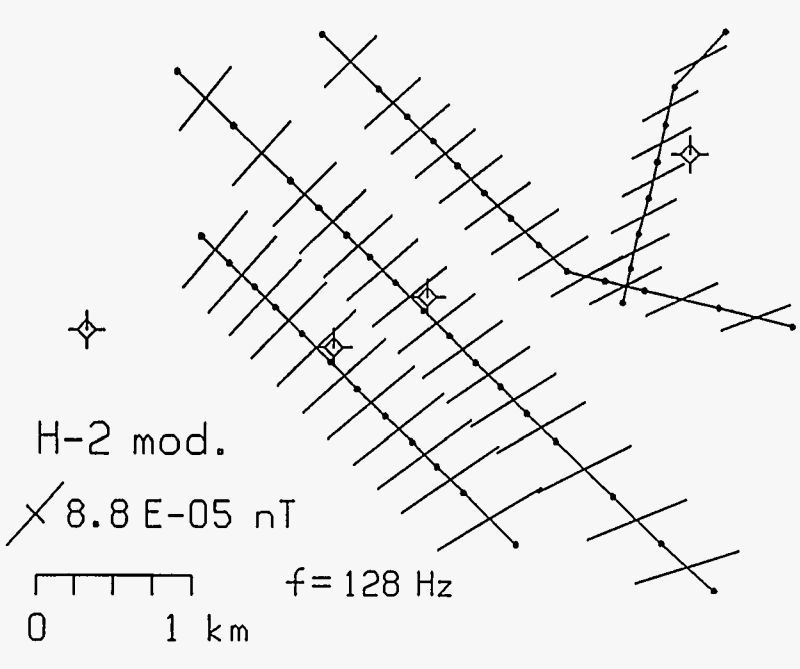
H-2 mod.
8.8 E-05 nT
f = 128 Hz
0
1 km

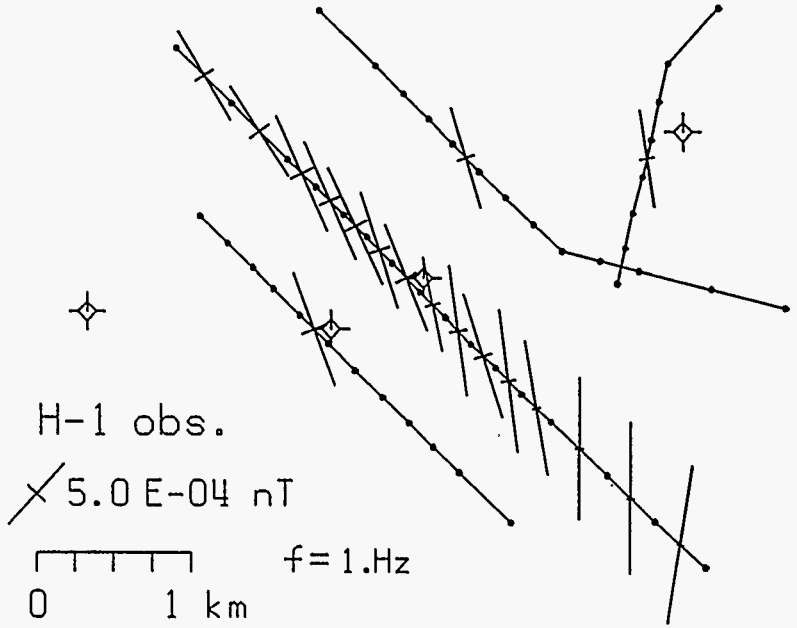
H-1 obs.
5.0 E-04 nT
f= 1.Hz
0
1 km

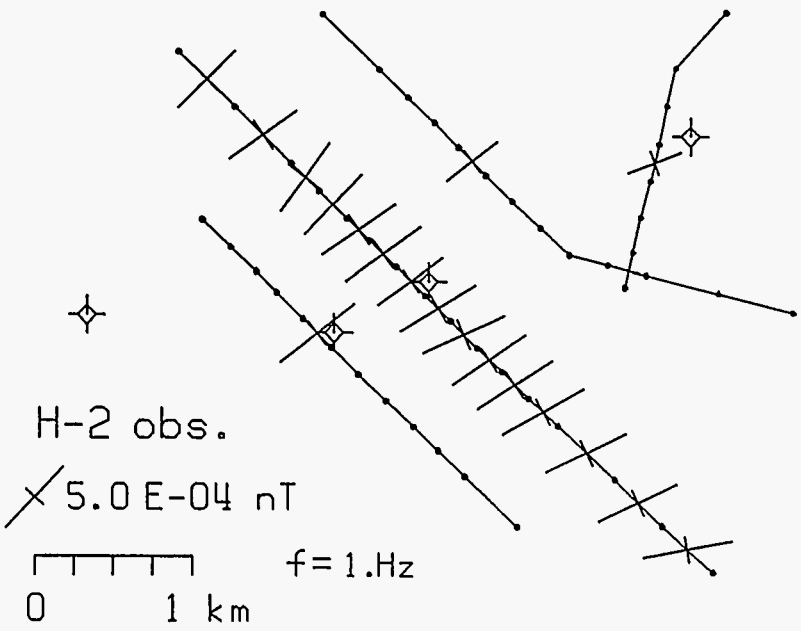
H-2 obs.
5.0 E-04 nT
f= 1.Hz
0
1 km

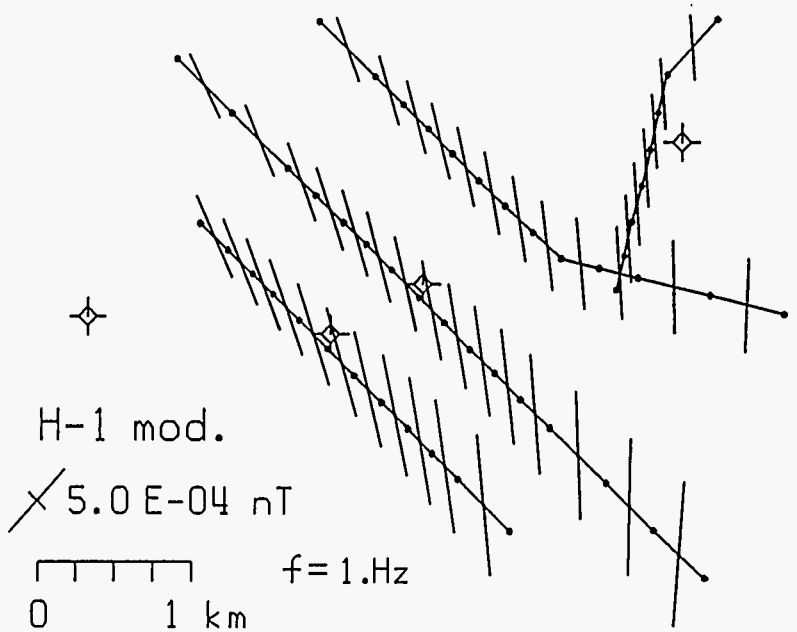
H-1 mod.
5.0 E-04 nT
f= 1.Hz
0
1 km

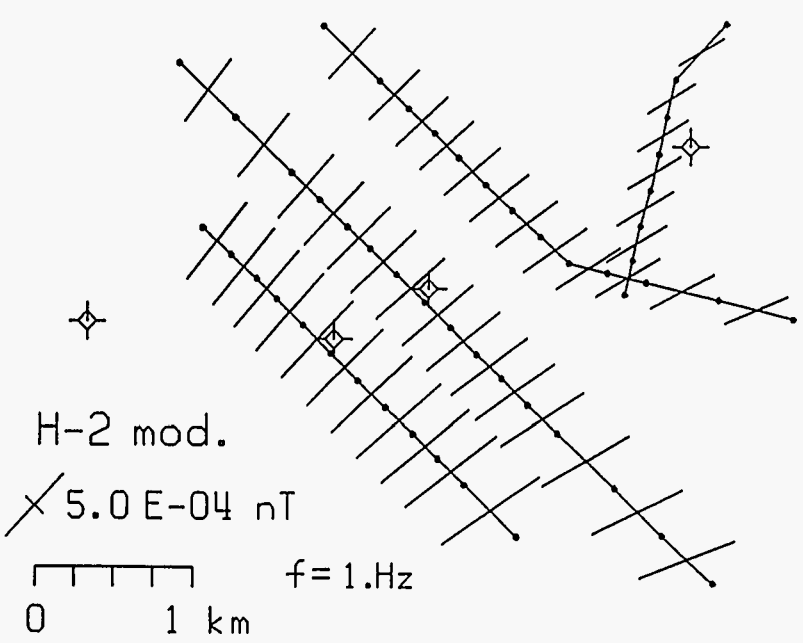
H-2 mod.
5.0 E-04 nT
f= 1.Hz
0
1 km

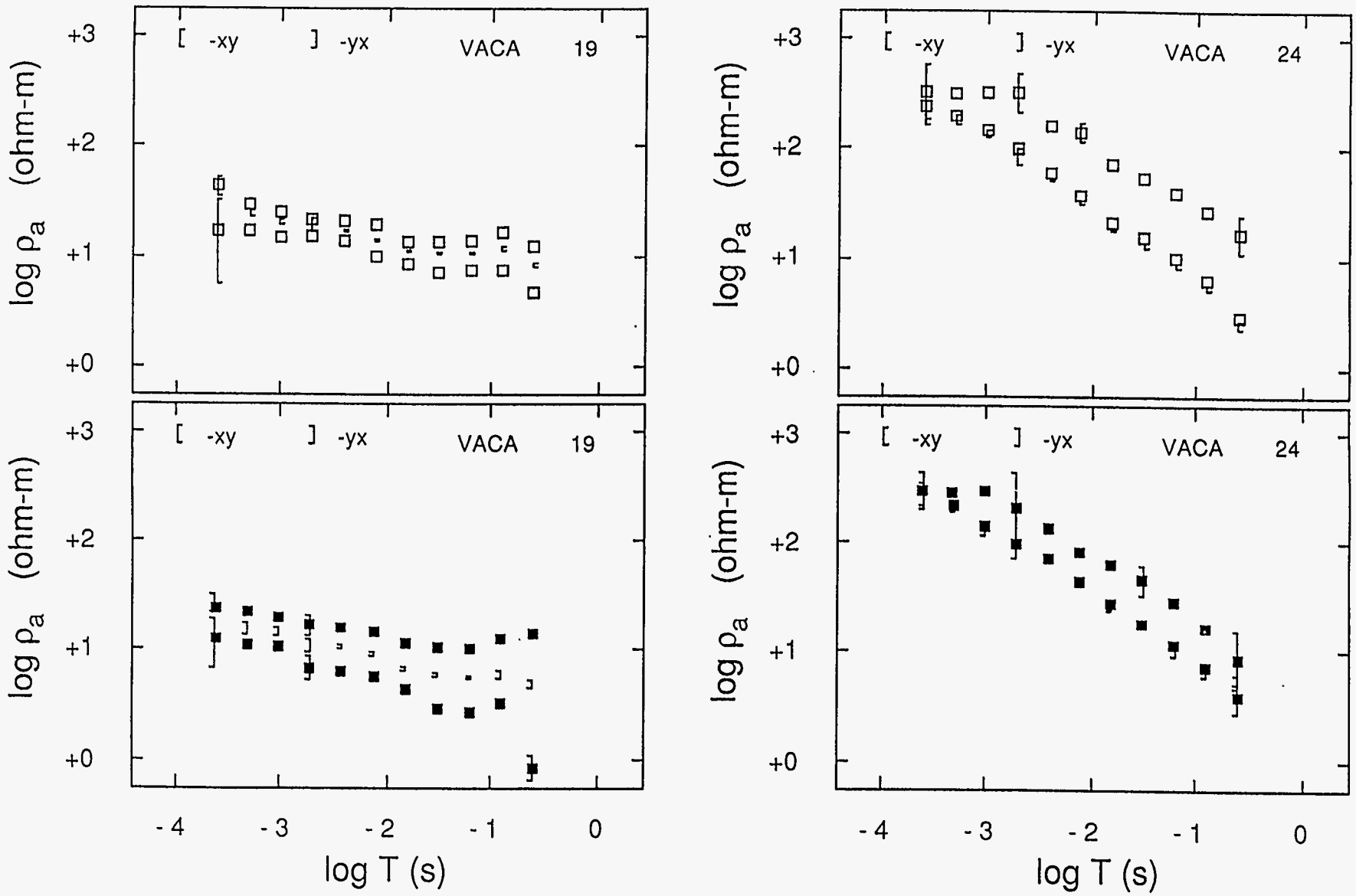
[ -xy
] -yx
VACA 19
VACA 24
log ρa (ohm-m)
+3
+2
+1
+0
- 4
- 3
- 2
- 1
0
log T (s)